Relaxation method for Mie-Grüneisen type equations of state

Loann Neron, Richard Saurel, Alexandre Chiapolino, François Fraysse

Relaxation method for Mie-Grüneisen type equations of state

Loann Neron [1,2,*], Richard Saurel [1,2], Alexandre Chiapolino [1] and François Fraysse [1]

[1] RS2N SAS, 371 chemin de Gaumin, 83640 Saint-Zacharie, France

[2] Aix Marseille Univ, CNRS, Centrale Marseille, LMA UMR 7031, Marseille, France

[*] Corresponding author: loann.neron@etu.univ-amu.fr, loann.neron@rs2n.eu

This paper is dedicated to the memory of Sergei Konstantinovich Godunov

Abstract

Mie-Grüneisen type equations of state (EOS) are widely used to describe the thermodynamics of solids, liquids, and gases in a variety of physics problems, including shock wave dynamics in condensed materials and the thermodynamic behavior of dense gases generated by detonation waves. The Jones-Wilkins-Lee (JWL), Cochran-Chan, and original Mie-Grüneisen EOSs are relevant examples. However, these EOSs present several major difficulties. First, their range of validity is limited because these EOSs are fitted to a reference curve and tolerate only small deviations from that curve. The second difficulty lies in the complexity of the mathematical formulations, affecting the efficiency of pressure relaxation solvers. These two difficulties give rise to a third. Under extreme flow conditions, computational failures are quite common. Methods for "extending" the equations of state are often used to continue the computations. For example, below a certain arbitrary density, the JWL EOS is sometimes extended to the ideal-gas EOS. A fundamentally new method is presented in this work. It consists of using the much simpler Noble-Abel-stiffened-gas EOS as a *predictor*, to close the corresponding flow model. A thermodynamic relaxation step follows the prediction step. The solution is projected onto the *target* EOS, in this case the Mie-Grüneisen EOS, with the help of additional transport equations. Therefore, the flow model is an extended version, much more efficient for numerical resolution. This method solves the three problems above by extending the validity domain of the thermodynamic formulation, making the relaxation solvers much faster, and dramatically increasing the robustness of computations.

Keywords: Equation of state; JWL; Relaxation; Convexity; Limited range of validity; Shock and detonation waves.

1. Introduction

Mie-Grüneisen (MG) (Mie, 1903 and Grüneisen 1912) equations of state (EOS) are widely used to describe the thermodynamics of solids, liquids, and gases in a variety of problems in physics, such as the propagation of shock waves in condensed materials (Marsh, 1980, Bushman et al., 2004, Levashov et al., 2004) and mixtures of them (Saurel et al., 2007a). When dealing with the detonation of condensed explosives, the Jones-Wilkins-Lee (JWL) EOS (Lee et al., 1968) seems to be the most popular formulation for engineering computations. In this area, many thermochemical codes have been developed, such as Cheetah (Fried et al., 1998) or EXPLO5 (Sućeska, 1999) to compute the JWL parameters from the isentrope emerging from the Chapman-Jouguet (CJ) point. The JWL EOS is then used in most computer codes under the Mie-Grüneisen form. See for example Souers et al. (2000), Chinnayya et al. (2004), Saurel et al. (2018), and many others. MG-type EOSs are also widely used for impact computations (Povarnitsyn et al., 2006, Lomonosov and Fortova, 2017). However, the MG EOS and its variants, such as the JWL EOS, present fundamental difficulties.

First, their range of validity is limited. This is due to the fact that these EOSs are fitted to a reference curve and tolerate only small deviations from it. When dealing with shock physics, the MG EOS and the Cochran and Chan (1979) variant, as well as reduced versions such as the stiffened-gas EOS and the Noble-Abel-stiffened-gas EOS (Le Métayer and Saurel, 2016) are fitted to the Hugoniot curve. This means that an isentropic expansion can be problematic when the amplitude of this process is large. When dealing with multiphase formulations, the phases are present everywhere and all kinds of thermodynamic transformations occur, such as compression, expansion, heating, and cooling. Therefore, domain restrictions are problematic. These restrictions appear as negative square sound speed, negative temperature, which are consequences of the lack of convexity of the formulation. Details about convexity can be found in Godunov et al. (1976), Menikoff and Plohr (1989), Neron and Saurel (2022). To overcome these difficulties, MG formulations are expanded to low density using a stiffened-gas formulation. Sometimes it is also necessary to perform a similar expansion at high density. The literature is lacking in this respect as these expansions involve a certain degree of arbitrariness. Some details can be found in Miller and Puckett (1996) and Arienti et al. (2004). The same difficulty arises with the JWL EOS. It is fitted to the isentrope emerging from the CJ point. But expansions far from this isentrope can occur, as well as heating and even re-shock. Sophisticated MG-type EOSs that are valid over a wide range of thermodynamic states exist, see for example Lomonosov and Fortova (2017), Belkheeva (2022). However, calibration of such EOSs requires extensive knowledge of the material properties, which may not always be available.

JWL and MG EOSs are generally convex, well-posed, and accurate in their domain of validity and fitting. However, they can hardly be used in computer codes, single-phase, multiphase, and diffuse-interface without extensions of their domain of validity and convexity. Such extensions introduce complexity in the formulation and are sometimes inefficient under extreme flow conditions. These problems are exacerbated in the context of multi-material and multiphase computations when pressure relaxation solvers are used (see for instance Le Métayer et al., 2013). For example, pressure relaxation solvers are required in the context of hyperbolic multiphase models (Baer and Nunziato, 1986) and diffuse-interface methods (Saurel and Abgrall, 1999a, Kapila et al., 2001, Udaykumar et al., 2003, Saurel and Pantano, 2018). As the various thermodynamic formulas are heavy, most of the computational time is spent in relaxation solvers and various thermodynamic subroutines. These two difficulties give rise to a third, which is related to the robustness of the computations. Under extreme flow conditions, computational failures are quite common. In this case, various methods are used to extend the EOS in order to continue the computations. Sometimes, temperature relaxation is used in addition to pressure relaxation, resulting in entropy production and computational stabilization.

In the present work, a fundamentally new method is introduced. It consists of the computation of the considered flow model, single-phase or multiphase, with its Mie-Grüneisen type EOS, by means of a method using a *predictor* EOS (PEOS) and a *target* EOS (TEOS). The solution is obtained after a two-step procedure. It is reminiscent of the method of Coquel and Perthame (1998) but differs at several levels.

In the first step, the Noble-Abel-stiffened-gas (NASG) EOS (Le Métayer and Saurel, 2016) is used. Indeed, it is the simplest formulation that includes all molecular effects present in matter: agitation, long-range attraction, and short-range repulsion. Its formal mathematical expression is also convenient, since it consists of a reduction of all existing EOSs, such as MG, as well as cubic formulations, such as the van der Waals (1873) one. In the first step, the flow model is extended with additional transport equations for the various parameters or functions of the PEOS and TEOS.

The first step is followed by a thermodynamic relaxation step, during which the solution is projected onto the target EOS, in this case the MG EOS. At this stage, the transported variables are reset so that both the PEOS and the TEOS are locally perfectly merged. Thus, the flow model is slightly larger due to the presence of additional transport equations, but its numerical resolution is much more efficient. Indeed, during the hyperbolic evolution, in the Riemann solver, and in the pressure relaxation solver, the simple and explicit PEOS (NASG) is used.

This method solves the three above-mentioned problems by extending the validity domain of the thermodynamic formulation, by making the relaxation solvers significantly faster, and by dramatically increasing the robustness of computations. With the present method, the MG EOS is neither extended, nor used outside its validity range. If a convexity problem occurs, the thermodynamic reset is deactivated, and the computations continue with the last PEOS parameters. These parameters are still transported but are not reset to the non-convex TEOS surface. The computations become very robust due to the large convexity domain of PEOS. Depending on the flow model and the flow conditions, speedups between 30% and 50% are observed with the new method compared to the conventional one.

The paper is organized as follows. The (target) TEOSs, consisting of specific forms of the MG EOS are reported in Section 2. They consist of the Cochran and Chan (1979) EOS and the JWL (Lee et al., 1968) EOS. The (predictor) PEOS (NASG) is recalled in Section 3. The extended flow model is presented in Section 4 in the context of single-phase compressible flows. It consists of the Euler equations supplemented by some transport equations. Computational examples are shown and discussed in Section 5. The method is extended to non-equilibrium Baer-and-Nunziato type (1986) and diffuse-interface (Saurel et al., 2009) multiphase flow models in Sections 6 and 7. A multi-D computational example is then presented. It consists of an underwater explosion situation involving the motion of material interfaces under extreme flow conditions. Conclusions are given in Section 8.

2. Target EOS (TEOS)

The target EOS (TEOS) refers to the thermodynamic model targeted by the relaxation method, whose objective is to reproduce the solutions of the considered flow model computed with the TEOS thermodynamic closure. In the present context, TEOS is of MG form. Two different MG-form TEOSs are considered as examples. First, the Cochran and Chan (1979) EOS (CC) is studied because its formulation is simpler. Then, the more sophisticated JWL EOS (Lee et al., 1968) is considered. The general formulation of MG (2.1) and the specific functions of CC (2.3) and JWL (2.4) are summarized below,

$$\begin{cases} P(v,e) = \dfrac{\Gamma}{v}\left(e - e_k(v)\right) + P_k(v), \\ P(v,T) = \dfrac{\Gamma C_v T}{v} + P_k(v), \\ e(v,T) = C_v T + e_k(v), \\ c^2(v,P) = v(\Gamma+1)\left(P - P_k(v)\right) - v^2 \dfrac{dP_k}{dv}. \end{cases} \tag{2.1}$$

The notations are conventional. The variables P, v, e, T, and c represent the pressure, the specific volume, the specific internal energy, the temperature, and the sound speed respectively. The parameters Γ and C_v represent the Grüneisen coefficient and the specific heat at constant volume respectively. The latter two are considered as constant parameters in this paper. The Γ and C_v coefficients are defined as,

$$\Gamma = v\left.\frac{\partial P}{\partial e}\right|_v, \qquad C_v = \left.\frac{\partial e}{\partial T}\right|_v. \tag{2.2}$$

Functions P_k and e_k are specific to the MG-type EOS under consideration. For the CC EOS, the various functions denoted by the subscript "CC" read,

$$\begin{cases} P_k(v) = P_{CC}(v) = A_1\left(\dfrac{v}{v_{ref}}\right)^{-E_1} - A_2\left(\dfrac{v}{v_{ref}}\right)^{-E_2}, \\ e_k(v) = e_{CC}(v) = -\dfrac{A_1 v_{ref}}{(1-E_1)}\left(\left(\dfrac{v}{v_{ref}}\right)^{1-E_1} - 1\right) + \dfrac{A_2 v_{ref}}{(1-E_2)}\left(\left(\dfrac{v}{v_{ref}}\right)^{1-E_2} - 1\right) - C_v T_{ref} + e_{ref}, \\ \dfrac{dP_k}{dv} = \dfrac{dP_{CC}}{dv} = -\dfrac{A_1 E_1}{v_{ref}}\left(\dfrac{v}{v_{ref}}\right)^{-1-E_1} + \dfrac{A_2 E_2}{v_{ref}}\left(\dfrac{v}{v_{ref}}\right)^{-1-E_2}, \end{cases} \tag{2.3}$$

where A_1, A_2, E_1, and E_2 are empirically adjusted parameters depending on the studied material. Subscript "ref" indicates the reference state data used to calibrate these parameters.

For the JWL EOS the various functions used in (2.1) are denoted by the subscript "JWL" and read,

$$
\begin{cases}
P_k(v) = P_{JWL}(v) = P_1(v) + k\left(\dfrac{v_{ref}}{v}\right)^{\Gamma+1}, \\
e_k(v) = e_{JWL}(v) = \dfrac{Av_{ref}}{R_1} e^{-R_1\frac{v}{v_{ref}}} + \dfrac{Bv_{ref}}{R_2} e^{-R_2\frac{v}{v_{ref}}} + \dfrac{kv_{ref}}{\Gamma}\left(\dfrac{v_{ref}}{v}\right)^{\Gamma} + e_{ref}, \\
\dfrac{dP_k}{dv} = \dfrac{dP_{JWL}}{dv} = -\dfrac{AR_1}{v_{ref}} e^{-R_1\frac{v}{v_{ref}}} - \dfrac{BR_2}{v_{ref}} e^{-R_2\frac{v}{v_{ref}}} - (1+\Gamma)\dfrac{kv_{ref}}{v^2}\left(\dfrac{v_{ref}}{v}\right)^{\Gamma}, \\
P_1(v) = Ae^{-R_1\frac{v}{v_{ref}}} + Be^{-R_2\frac{v}{v_{ref}}}, \\
k = \left(P_{CJ} - P_1(v_{CJ}) - \dfrac{\Gamma C_v T_{CJ}}{v_{CJ}}\right)\left(\dfrac{v_{CJ}}{v_{ref}}\right)^{\Gamma+1} = C - \dfrac{\Gamma C_v T_{CJ}}{v_{CJ}}\left(\dfrac{v_{CJ}}{v_{ref}}\right)^{\Gamma+1}, \\
e_{ref} = e_{CJ} - \dfrac{Av_{ref}}{R_1} e^{-R_1\frac{v_{CJ}}{v_{ref}}} - \dfrac{Bv_{ref}}{R_2} e^{-R_2\frac{v_{CJ}}{v_{ref}}} - v_{CJ}\dfrac{P_{CJ} - P_1(v_{CJ})}{\Gamma}, \\
v_{CJ} = v_{ref} - P_{CJ}\left(\dfrac{v_{ref}}{D_{CJ}}\right)^2, \\
e_{CJ} = \dfrac{p_{CJ}}{2}(v_{ref} - v_{CJ}),
\end{cases}
\tag{2.4}
$$

where A, B, C, R_1, R_2, and k are fitted parameters depending on the considered material. The subscript "ref" and "CJ" denote the reference state and Chapman-Jouguet state respectively, which are used to fit the parameters.

The EOS (2.1) is therefore the target EOS to be solved. However, the complexity of the TEOS formulations, both with CC and even more with JWL, is the main motivation for the relaxation approach developed in the present work. Moreover, these EOSs have a limited domain of validity, which makes the whole computation difficult. The target EOS is therefore treated with a simpler dummy EOS, typically of the NASG form. The dummy EOS acts as a predictor for the thermodynamic variables with the aim of recovering the state associated with the target EOS.

3. Predictor EOS (PEOS)

The Predictor EOS (PEOS) refers to the simplified thermodynamic model whose goal is to recover the thermodynamic state of the target model, at least locally at a given thermodynamic point. The Noble-Abel-stiffened-gas (NASG) EOS is chosen because it is the simplest formulation that includes the three molecular forces present in matter (agitation, short-range repulsion, and long-range attraction). More sophisticated EOS can be expressed in the NASG form, with more or less complex functions instead of the constants present in this EOS. Its formal expression is therefore convenient as a local reduced formulation for all other existing analytical formulations. Moreover, the NASG EOS is convex over a wide range of thermodynamic states. The various formulations of NASG are summarized in (3.1),

$$\begin{cases} P(v,e) = \dfrac{(\gamma^*-1)(e-q^*)}{v-b^*} - \gamma^* P_\infty^* = \dfrac{R^*(e-q^*)}{C_v^*(v-b^*)} - \left(\dfrac{R^*}{C_v^*}+1\right)P_\infty^*, \\ P(v,T) = \dfrac{(\gamma^*-1)C_v^* T}{v-b^*} - P_\infty^* = \dfrac{R^* T}{v-b^*} - P_\infty^*, \\ e(v,T) = C_v^* T + P_\infty^*(v-b^*) + q^*, \\ c^2(v,P) = \dfrac{\gamma^* v^2 (P+P_\infty^*)}{v-b^*} = \dfrac{v^2 (R^*+C_v^*)(P+P_\infty^*)}{C_v^*(v-b^*)}. \end{cases} \tag{3.1}$$

The thermodynamic parameters marked with a star * represent the parameters that are to be adapted to match the TEOS formulation. In the NASG (PEOS) relations (3.1), C_v^* remains the specific heat at constant volume. The parameter b^* represents the covolume, modeling short-range repulsive effects. The parameter P_∞^* represents attractive ones, present only in condensed matter, and q^* is the formation (or reference) internal energy. Finally, the specific gas constant $R^* = (\gamma^*-1)C_v^*$ with γ^* the adiabatic coefficient, is associated with thermal agitation and results from the thermodynamic relation of Mayer, as detailed in Appendix A.

The NASG EOS (3.1) is convex as long as $P > -P_\infty^*$ thus guaranteeing a quite large range of convexity. The adjustment of these parameters is done later through functions depending on the internal energy and the specific volume in order to match the various thermodynamic variables between TEOS and PEOS.

Comparing TEOS (2.1) and PEOS (3.1), these EOSs appear quite different. To determine the thermodynamic state corresponding to the target TEOS, the flow model is modified. Additional equations are added for each of the thermodynamic parameters of PEOS. These equations address transport as well as relaxation of the thermodynamic parameters marked with a star. It means that each equation added for the PEOS parameters address transport of the corresponding parameter in the flow and a relaxation term is present in each equation to locally recover the TEOS predictions. After transport, instantaneous thermodynamic relaxation is achieved, so that TEOS and PEOS are locally merged.

4. Hyperbolic formulation with relaxation

The method is presented in this section in the single-phase context of the 1D Euler equations of gas dynamics. Five additional transport equations are added, one for each of the thermodynamic parameters of the PEOS: b^*, P_∞^*, R^*, C_v^*, and q^*. These transport equations are written under conservative form, with the help of mass conservation,

$$\begin{cases} \dfrac{\partial \rho}{\partial t} + \dfrac{\partial \rho u}{\partial x} = 0, \\ \dfrac{\partial \rho u}{\partial t} + \dfrac{\partial (\rho u^2 + P)}{\partial x} = 0, \\ \dfrac{\partial \rho E}{\partial t} + \dfrac{\partial (\rho E + P)u}{\partial x} = 0, \end{cases} \tag{4.1}$$

$$\begin{cases} \dfrac{\partial \rho b^*}{\partial t} + \dfrac{\partial \rho b^* u}{\partial x} = \dfrac{\rho}{\tau}\left(b(v,e) - b^*\right), \\ \dfrac{\partial \rho P_\infty^*}{\partial t} + \dfrac{\partial \rho P_\infty^* u}{\partial x} = \dfrac{\rho}{\tau}\left(P_\infty(v,e) - P_\infty^*\right), \\ \dfrac{\partial \rho R^*}{\partial t} + \dfrac{\partial \rho R^* u}{\partial x} = \dfrac{\rho}{\tau}\left(R(v,e) - R^*\right), \\ \dfrac{\partial \rho C_v^*}{\partial t} + \dfrac{\partial \rho C_v^* u}{\partial x} = \dfrac{\rho}{\tau}\left(C_v(v,e) - C_v^*\right), \\ \dfrac{\partial \rho q^*}{\partial t} + \dfrac{\partial \rho q^* u}{\partial x} = \dfrac{\rho}{\tau}\left(q(v,e) - q^*\right), \\ \text{with } \tau \to 0^+ \text{ when the convexity relations } \left(\text{see Section 4.4 } (4.15)\right) \text{ are fulfilled, otherwise } \tau \to +\infty. \end{cases} \tag{4.2}$$

System (4.1-4.2) forms the extended flow model with the transport-relaxation equations (4.2). Its thermodynamic closure is achieved with (3.1). The notations are conventional. Most of the notations have already been defined with (2.1). In addition, $\rho = \dfrac{1}{v}$, u, and $E = e + \dfrac{1}{2}u^2$ denote the density, the velocity, and the total energy respectively. The thermodynamic parameters with a star symbol are used in PEOS (3.1). Each equation in (4.2) contains a relaxation term. The various functions $b(v,e)$, $P_\infty(v,e)$, $R(v,e)$, $C_v(v,e)$, and $q(v,e)$ are constructed in such a way that TEOS and PEOS merge in the limit $\tau \to 0^+$. As examined in Section 4.4, instantaneous relaxation ($\tau \to 0^+$) is done only when the convexity conditions are fulfilled. Otherwise, no relaxation is done, meaning that the relaxation terms of (4.2) are removed, *i.e.*, $\tau \to +\infty$. The relaxation rate τ is defined in these two limits only, meaning that no finite rate relaxation is used. Stiff relaxation of the thermodynamic parameters guarantees that the extended System (4.1-4.2) tends to the target model which is System (4.1) thermodynamically closed with TEOS.

System (4.1-4.2) corresponds to an extended hyperbolic system with stiff relaxation. It appears more convenient for numerical resolution than the original Euler equations with the target EOS (MG in the article). It is more convenient at computational level, faster, and the prolongation outside the range of convexity is automatic, maintaining hyperbolicity of the formulation. This property is lost with the Euler equations and TEOS when convexity conditions are violated.

Extended hyperbolic systems are now widely used in various areas of physics and numerics. Relevant references are for example Chen et al. (1994), Levermore (1996), Coquel and Perthame (1998), Saurel and Abgrall (1999b), Kapila et al. (2001), Saurel et al. (2009), Lund (2012).

System (4.1-4.2) is built in order that it is hyperbolic with wave speeds u, $u + c$, and $u - c$, where the sound speed c is given by (3.1). Asymptotic considerations, given later in Section 4.3, show that this extended system matches the target system, with TEOS. System (4.1-4.2) is solved in the absence of relaxation terms during a time step with the user's favorite scheme. In the present paper the Godunov (1959) method is used with the HLLC (Harten-Lax-van Leer-Contact) Riemann solver of Toro et al. (1994) for the computation of the hyperbolic step (computation of System (4.1-4.2) without source terms). After the hyperbolic step, stiff relaxation is achieved to merge TEOS and PEOS.

Some remarks are necessary first. In the present context, since TEOS is of MG type, covolume effects are absent: $b^* = 0$. This means that the first equation of (4.2) is removed. This is not true when considering cubic EOSs such as those of van der Waals type. However, non-convex cubic EOSs pose additional difficulties, such as modeling phase transitions, which are beyond the scope of the present

work. Second, the thermodynamic parameters R^* and C_v^* are linked through the relation of Mayer as detailed in Appendix A,

$$C_v^* = \frac{R^*}{\Gamma}. \tag{4.3}$$

This means that another equation can be removed from System (4.2). Thus, only 3 coefficients remain to be determined: R^*, P_∞^*, and q^*.

These coefficients are determined to satisfy the three conditions:

$$\begin{cases} P_{TEOS}(v,e) = P_{PEOS}(v,e), \\ T_{TEOS}(v,e) = T_{PEOS}(v,e), \\ c^2{}_{TEOS}(v,e) = c^2{}_{PEOS}(v,e). \end{cases} \tag{4.4}$$

Note that the specific volume v and internal energy e are provided by the flow model (System (4.1) in this section), regardless of the equation of state. It is also worth mentioning that the equality of the square sound speeds involves the equality of the partial derivatives,

$$\left.\frac{\partial P_{TEOS}}{\partial \rho}\right|_s = \left.\frac{\partial P_{PEOS}}{\partial \rho}\right|_s, \tag{4.5}$$

where s is the specific entropy. In addition, through Relation (4.3), the following partial derivatives are equated as well,

$$\left.\frac{\partial P_{TEOS}}{\partial e}\right|_v = \left.\frac{\partial P_{PEOS}}{\partial e}\right|_v, \tag{4.6}$$

as detailed in Appendix A. This means that the same Grüneisen coefficient is used in both PEOS and TEOS.

With the help of the PEOS equations (3.1), the solution to System (4.4) reads,

$$\begin{cases} R^* = \dfrac{c^2{}_{TEOS}(v,e)}{(\Gamma+1)T_{TEOS}(v,e)}, \\ P_\infty^* = \dfrac{c^2{}_{TEOS}(v,e)}{v(\Gamma+1)} - P_{TEOS}(v,e), \\ q^* = e - \dfrac{c^2{}_{TEOS}(v,e)}{\Gamma} + vP_{TEOS}(v,e). \end{cases} \tag{4.7}$$

Alternatively, introducing the TEOS expressions (2.1) in (4.7), the following relations appear,

$$\begin{cases} R^* = \Gamma C_v - \dfrac{v^2 C_v}{(\Gamma+1)\left(e - e_k(v)\right)} \dfrac{dP_k}{dv}, \\ P_\infty^* = -P_k(v) - \dfrac{v}{\Gamma+1}\dfrac{dP_k}{dv}, \\ q^* = e_k(v) + vP_k(v) + \dfrac{v^2}{\Gamma}\dfrac{dP_k}{dv}. \end{cases} \tag{4.8}$$

Relations (4.8) are used to reset the three thermodynamic parameters R^*, P_∞^*, and q^* before the next time step, *i.e.*, before the next hyperbolic-transport step.

4.1. Sub-characteristic condition

Another remark is worth mentioning. As System (4.1-4.2) is a non-equilibrium flow model when PEOS is used instead of TEOS, the sub-characteristic condition of Liu (1987) must be satisfied. Here it corresponds to,

$$c^2_{PEOS} \geq c^2_{TEOS}. \tag{4.9}$$

This condition is automatically satisfied during the relaxation step by the last equation of (4.4).

4.2. Summary

In the frame of the present contribution, as the target EOS is of MG type, where covolume effects are absent, and as parameters R^* and C_v^* are linked through Relation (4.3), the flow model consists of (4.1) complemented by:

$$\begin{cases} \dfrac{\partial \rho P_\infty^*}{\partial t} + \dfrac{\partial \rho P_\infty^* u}{\partial x} = \dfrac{\rho}{\tau}\left(P_\infty(v) - P_\infty^*\right), \\ \dfrac{\partial \rho R^*}{\partial t} + \dfrac{\partial \rho R^* u}{\partial x} = \dfrac{\rho}{\tau}\left(R(v,e) - R^*\right), \\ \dfrac{\partial \rho q^*}{\partial t} + \dfrac{\partial \rho q^* u}{\partial x} = \dfrac{\rho}{\tau}\left(q(v) - q^*\right), \\ \text{with } \tau \to 0^+ \text{ when the convexity relations } \left(\text{see Section 4.4 } (4.15)\right) \text{ are fulfilled, otherwise } \tau \to +\infty. \end{cases} \tag{4.10}$$

The EOS used during the hyperbolic step is (3.1) and the relaxation step is done with Relations (4.8).

4.3. Asymptotic considerations

Another remark may help to analyze this relaxation method. For the sake of simplicity let us consider the first equation of System (4.10) as P_∞ is dependent on a single variable: $P_\infty(v)$. The lagrangian derivative is denoted as,

$$\frac{d}{dt} = \frac{\partial}{\partial t} + u\frac{\partial}{\partial x}.$$

As P_∞ depends on the specific volume, its evolution over time is given by,

$$\frac{dP_\infty}{dt} = \frac{dP_\infty}{dv}\frac{dv}{dt}. \tag{4.11}$$

The first equation of System (4.10) is then combined with the mass equation of System (4.1). The following result is readily obtained:

$$\frac{\partial P_\infty^*}{\partial t} + u\frac{\partial P_\infty^*}{\partial x} = \frac{P_\infty(v) - P_\infty^*}{\tau}. \tag{4.12}$$

Let us now consider a first-order Taylor expansion of $P_\infty(v)$ around the initial specific volume v_0:

$$P_\infty(v) \cong P_\infty(v_0) + (v - v_0)\frac{dP_\infty}{dv}.$$

Inserting this result in (4.12) yields,

$$\frac{\partial P_\infty^*}{\partial t} + u\frac{\partial P_\infty^*}{\partial x} = \frac{P_\infty(v_0) + (v - v_0)\dfrac{dP_\infty}{dv} - P_\infty^*}{\tau}. \tag{4.13}$$

As $P_\infty^* \cong P_\infty(v_0)$ from the preceding relaxation step, (4.13) becomes,

$$\frac{\partial P_\infty^*}{\partial t} + u\frac{\partial P_\infty^*}{\partial x} = \frac{dP_\infty}{dv}\frac{(v - v_0)}{\tau}. \tag{4.14}$$

In the asymptotic limit when $\tau \to 0^+$, (4.14) tends to (4.11). As (4.11) is an exact formula from TEOS, the relaxation method based on (4.14) and PEOS tends to the exact formula (4.11), provided that $\tau \to 0^+$, which is the case for numerical methods where wave propagation is considered. Stiff relaxation ($\tau \to 0^+$) is done when the convexity conditions are fulfilled, as examined hereafter.

4.4. Relaxation switch

When the relaxation step (4.8) is achieved, asymptotic considerations show that the flow model with PEOS tends to the solutions of TEOS. The numerical experiments reported in the next section confirm this observation. However, TEOS is sometimes inappropriate, in the sense that its domain of validity is limited. Such a situation is quite common in multiphase and diffuse-interface computations as the fluids are present everywhere, sometimes in very small proportions, and subjected to variations dictated by another phase. For example, a solid phase may be present as a continuum medium in a very small volume fraction, in an expanding fluid in large proportions. The normal behavior of the solid phase in such an expansion is not to remain continuous. In fact, such material does not exist in reality, but the computation and the theoretical formulation must manage its presence, in vanishing proportions.

When the TEOS is used outside its domain of validity, convexity problems arise. Details about convexity and various forms for convexity expressions are available in Godunov et al. (1976), Menikoff and Plohr (1989), Chiapolino and Saurel (2018), Neron and Saurel (2022). Using the method described in Appendix B, the following convexity criteria are derived for the MG EOS,

$$\begin{cases} P > P_k(v) + \dfrac{v}{\Gamma + 1}\dfrac{dP_k}{dv}, \\ P > P_k(v), \\ P > P_k(v) + v\dfrac{dP_k}{dv}. \end{cases} \tag{4.15}$$

The convexity criteria (4.15) are valid for any MG formulation that satisfies $P_k(v) = -\dfrac{de_k}{dv}$. If the criteria (4.15) are not satisfied, the TEOS is out of its convexity range, which usually leads to incorrect predictions and possible computational failure (negative square sound speed or negative temperature). As mentioned in the Introduction, to avoid such difficulties, MG EOSs are sometimes extended with another EOS, such as the stiffened-gas EOS, with a certain degree of arbitrariness.

It should be noted that algebraic manipulations of the MG relations (2.1) result in,

$$\begin{cases} P - P_k(v) - \dfrac{v}{\Gamma+1}\dfrac{dP_k}{dv} = \dfrac{c^2}{v(\Gamma+1)}, \\ P - P_k(v) = \dfrac{\Gamma C_v T}{v}, \\ P - P_k(v) - v\dfrac{dP_k}{dv} = \dfrac{\Gamma C_v}{\beta v} = \dfrac{1}{\beta_T}, \end{cases} \tag{4.16}$$

where $\beta = \frac{1}{v}\frac{\partial v}{\partial T}\Big|_P$ and $\beta_T = -\frac{1}{v}\frac{\partial v}{\partial P}\Big|_T$ are the thermal expansion coefficient and the isothermal compressibility coefficient respectively. As the $\Gamma = v\frac{\partial P}{\partial e}\Big|_v$ and $C_v = \frac{\partial e}{\partial T}\Big|_v$ parameters are necessarily positive, the comparison between (4.15) and (4.16) reveals that the first condition of the convexity criteria (4.15) ensures a positive square sound speed c^2. The second condition ensures a positive temperature T. The third condition ensures a positive thermal expansion coefficient β and a positive isothermal compressibility coefficient β_T. The convexity criteria (4.15) consequently describe a thermodynamically stable equation of state (Menikoff, 2015).

With the proposed method, if the convexity criteria (4.15) are violated, the thermodynamic reset is switched off and the computations continue with the last PEOS parameters. These parameters are still transported by the flow but are not relaxed to the non-convex TEOS state. This means that the relaxation time in (4.10) now tends to infinity: $\tau \to +\infty$. Since the convexity domain of the PEOS (NASG), is much larger, the computations become very robust. This method automatically extends the MG EOS and guarantees continuity of all thermodynamic variables.

With the full relaxation method now available, various test problems are considered to assess the method, from 1D single-phase to 2D multiphase flows. The following three main points are addressed:

- Ability to catch the target thermodynamic state,
- Improved robustness,
- Computational time saving.

5. Single phase 1D results

In this section, the relaxation method is assessed on several test problems. First, the thermodynamic relaxation method described in Section 4 for the Euler equations is investigated using shock-tube and double-expansion test problems. The presentation discusses the ability of the predictor EOS to recover the results of the target EOS and its capability to compute a local convex state. This enables the computation with PEOS to continue when the conventional method (TEOS) fails. Second, the thermodynamic relaxation method is investigated in the frame of underwater explosions with a lagrangian scheme, further demonstrating the ability and robustness of the thermodynamic relaxation method compared to the conventional method based on TEOS.

5.1. Shock-tube tests

The flow model (4.1) extended by the transport-relaxation equations (4.10) is solved numerically with a Godunov-type method using the HLLC approximate Riemann solver to compute the intercell flux (Toro et al., 1994, Toro, 1999). After the hyperbolic step, the MG convexity conditions (4.15) are checked in each cell with the updated density and pressure. If the convexity criteria are fulfilled, the

thermodynamic parameters are instantaneously relaxed with relations (4.8). Otherwise, the relaxation step is omitted, and the thermodynamic parameters are only transported.

All computations are first-order in both space and time, to avoid any additional numerical component. The time step is computed with a CFL (Courant-Friedrichs-Lewy) criterion of 0.8. The computational domain is 1-m long and is spatially resolved with 500 cells. For each test case, the results obtained with the relaxation method (denoted as PEOS) are compared with the predictions obtained with the conventional method (denoted as TEOS) that uses the MG EOS to provide thermodynamic closure to System (4.1). The main objective is to ensure that both methods give the same results, *i.e.*, that the relaxation method is able to reproduce the results of the target model as expected. Shock-tube tests are considered to assess the method when discontinuities are present. Double-expansion tests are also considered to examine the relaxation method in the limit where the conventional method fails, when TEOS falls outside its validity range. Both CC and JWL formulations are considered. The corresponding thermodynamic parameters are summarized in Table I.

CC parameters (nitromethane)		**JWL parameters (TNT)**	
Γ	1.190	Γ	0.290
$C_v\ (J/kg/K)$	2000	$C_v\ (J/kg/K)$	2399
$A_1\ (GPa)$	0.819181	$A\ (GPa)$	492.6
$A_2\ (GPa)$	1.50835	$B\ (GPa)$	5.950
E_1	4.52969	$C\ (GPa)$	0.924
E_2	1.42144	R_1	4.730
$\rho_{ref}\ (kg/m^3)$	1134	R_2	1.060
$T_{ref}\ (K)$	300	$\rho_{ref}\ (kg/m^3)$	1605
$e_{ref}\ (J/kg)$	0	$D_{CJ}\ (m/s)$	6737
		$P_{CJ}\ (GPa)$	18.18
		$T_{CJ}\ (K)$	3712

Table I. Cochran-Chan (CC) parameters for liquid nitromethane and Jones-Wilkins-Lee (JWL) parameters for TNT detonation products taken from Saurel et al. (2007b) and Massoni et al. (2006) respectively.

All tests are initialized at a given pressure and a given density. When the relaxation method is used, the thermodynamic parameters of Equations (4.10) are initialized with Relations (4.8). To do this, the specific energy is required. Initially, the specific energy of the predictor model is assumed to be equal to the one of the target model and is computed with the MG formulation $e_{TEOS}(v,P)$ through Relations (2.1).

First, a shock-tube test with the CC EOS taken from Saurel et al. (2007b) is considered. The left chamber is initially set at high pressure $P = 200\,000$ bars and $\rho = 2000\ kg/m^3$. The right chamber is set at atmospheric pressure $P = 1$ bar and $\rho = 1134\ kg/m^3$. The initial discontinuity is located at 0.6 m. The computed results for both the conventional method (TEOS) and the relaxation method (PEOS) are shown in Figure 1 at time 70 μs.

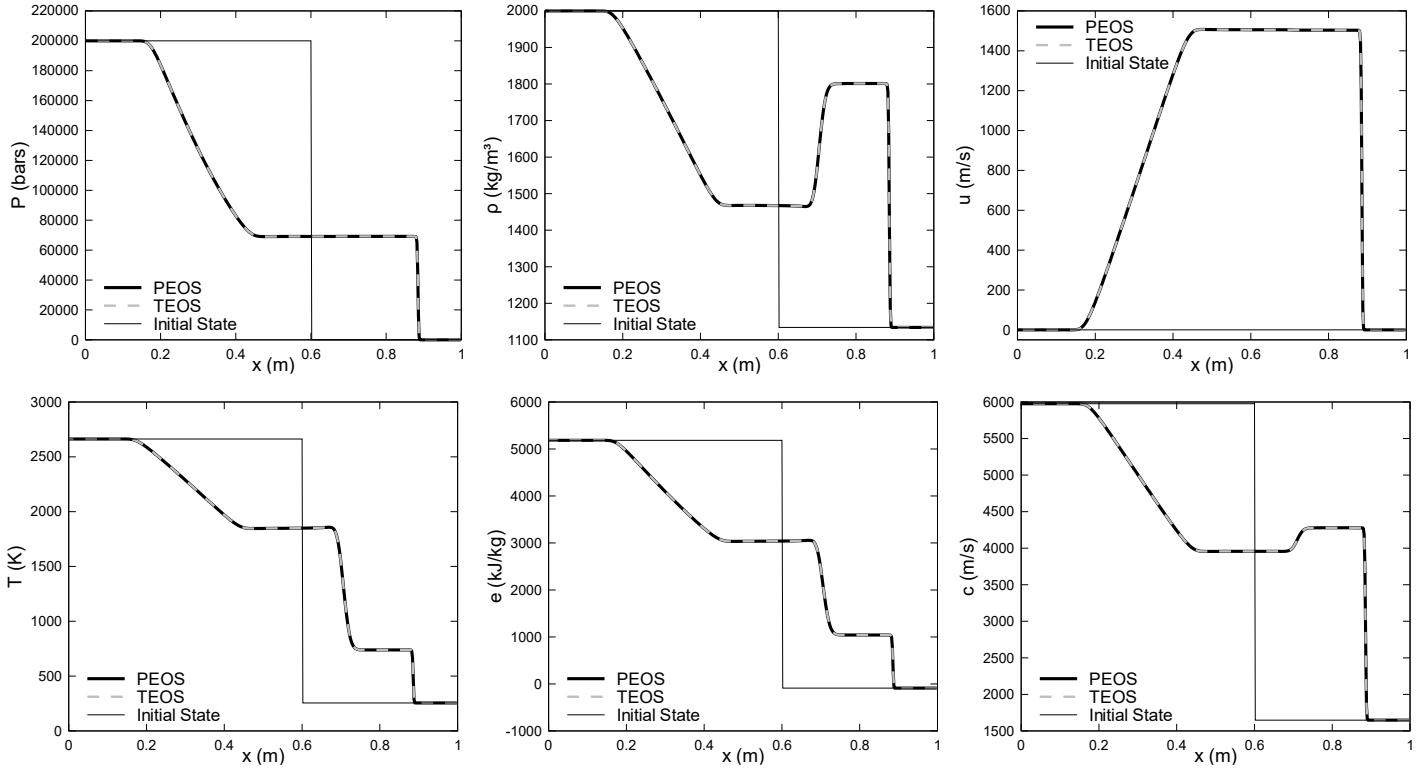

Figure 1. Single-phase shock-tube test case with the CC EOS. Dashed gray lines represent computed results with the conventional method (TEOS), and black lines correspond to the relaxation method (PEOS). Thin black lines represent the initial conditions. Results are shown at time 70 μs. The results of both methods are merged. The present relaxation method perfectly matches the target EOS.

The results obtained with the relaxation method using PEOS are in perfect agreement with those obtained with the conventional method using TEOS. At this stage, the new method seems to work nicely and as expected for the CC formulation. The computed PEOS parameters R^*, C_v^*, P_∞^*, and q^* are shown in Figure 2.

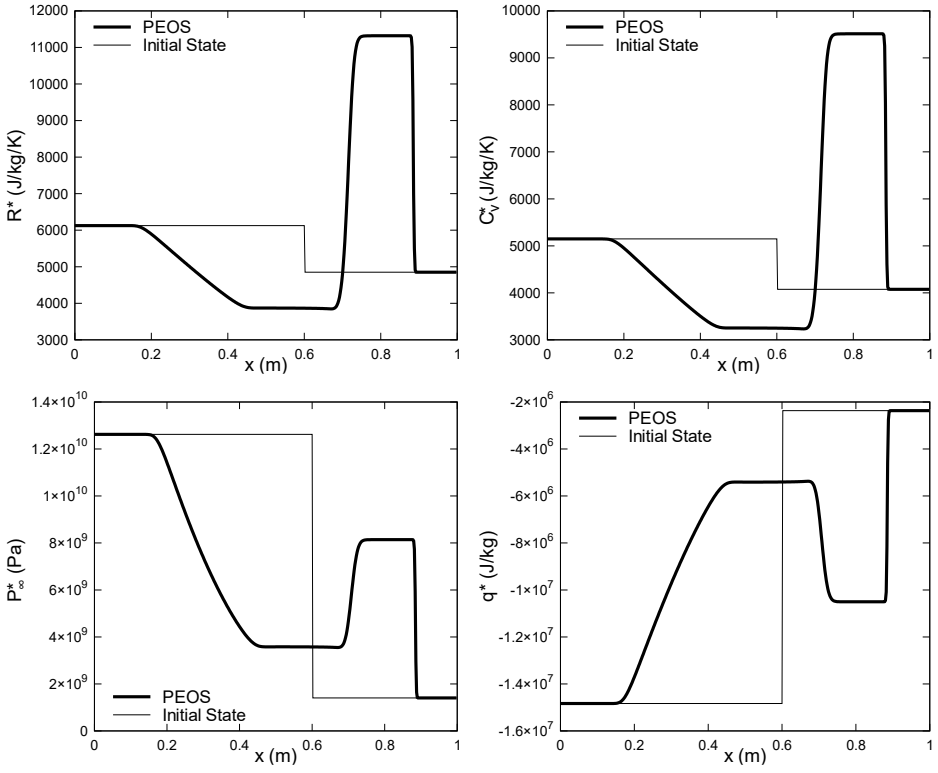

Figure 2. Single-phase shock-tube test case with the CC EOS. The thermodynamic parameters R^*, C_v^* P_∞^*, and q^* of the predictor EOS used to recover the target EOS solution in Figure 1, are shown. Thick lines represent the computed parameters at time 70 μs. The initial parameters are depicted in thin lines. Parameter b^* is not plotted since its value is set to zero.

The profile of the PEOS parameters follows the trend of the thermodynamic variables of Figure 1, specifically the trend of density. These parameters have no physical signification as the physical thermodynamic model under consideration is the TEOS. For example, the specific heat C_v^* does not correspond to the real specific heat of the material C_v, which is defined for the MG EOS.

A similar shock-tube test is considered for the JWL formulation. The left chamber is set at high pressure $P = 200\,000$ bars and $\rho = 2200\ \mathrm{kg/m^3}$. The right chamber is set at atmospheric pressure $P = 1$ bar and $\rho = 1000\ \mathrm{kg/m^3}$. The computed results are shown in Figure 3 at time 70 μs.

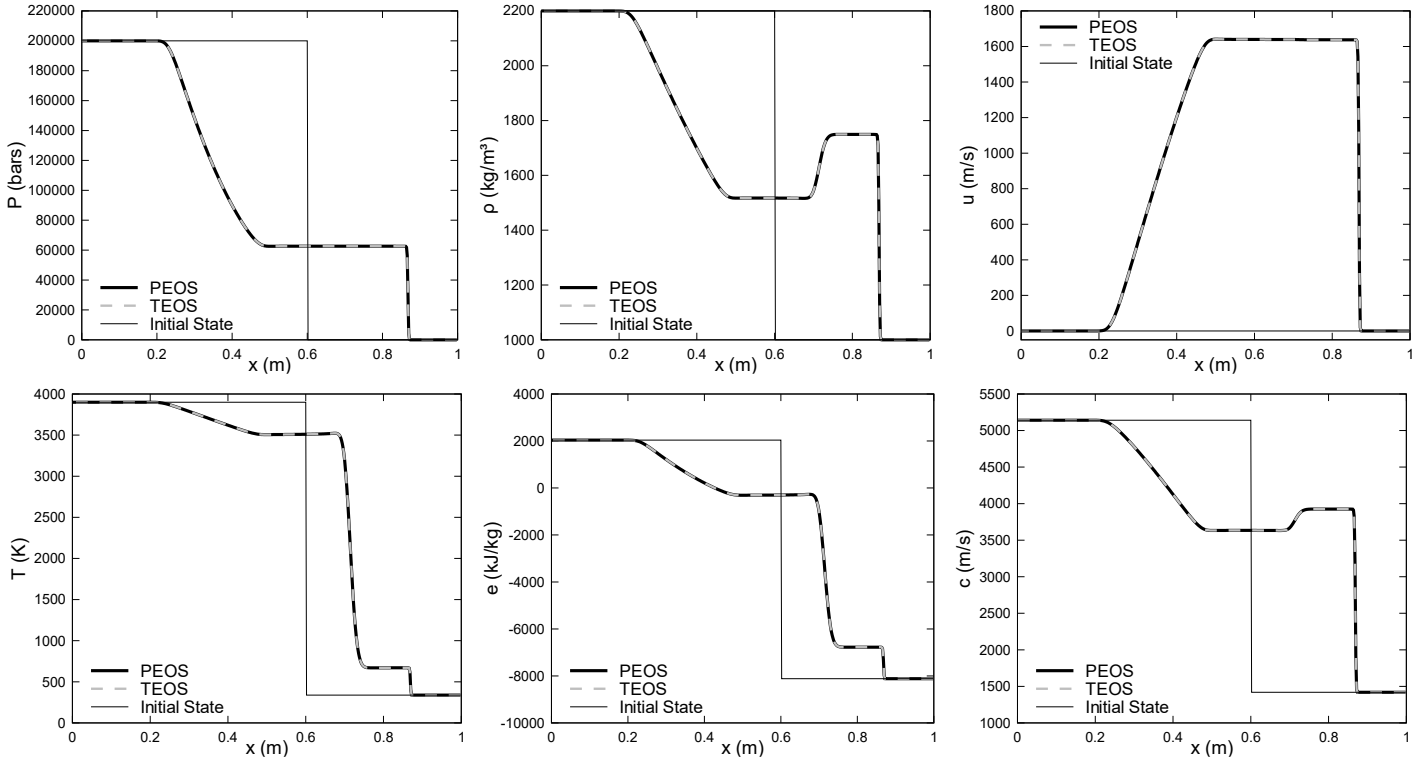

Figure 3. Single-phase shock-tube test case with the JWL EOS. Dashed gray lines represent computed results with the conventional method (TEOS), and black lines correspond to the relaxation method (PEOS). Thin black lines represent the initial conditions. Results are shown at time 70 μs. The results of both methods are merged. The present relaxation method recovers the target EOS results.

Again, the relaxation method computes the same results as the conventional method, with the JWL EOS. Since the relaxation method captures the results of the TEOS, the next step is to investigate the method in the limit where the conventional method fails.

5.2. Double-expansion tests

Double-expansion tests are now considered to assess the robustness of the relaxation method against conventional computations. In such tests, the fluid expands, and the density decreases significantly. The thermodynamic state eventually leaves the validity domain of the MG EOS, as indicated by the convexity criteria (4.15). Double expansion is reminiscent of vacuum formation, which often occurs under extreme multiphase flow situations such as underwater explosions. Vacuum treatment is one of the main sources of numerical difficulties with vanishing phases coming out of their range of validity. The main goal with double-expansion tests is to study the behavior of the relaxion method in situations where the conventional method fails. If the MG convexity criteria are violated, the relaxation of the thermodynamic parameters with the PEOS is switched off. The computations continue with the NASG EOS, which has a much larger range of validity.

The first double-expansion test is achieved with the CC formulation. The domain is initially set at $P = 1$ bar and $\rho = 1134\ \mathrm{kg/m^3}$ with an expansion velocity of ± 200 m/s. The initial discontinuity is located at 0.5 m. Both methods successfully compute the corresponding flow. Results are shown in Figure 4 at time 200 μs.

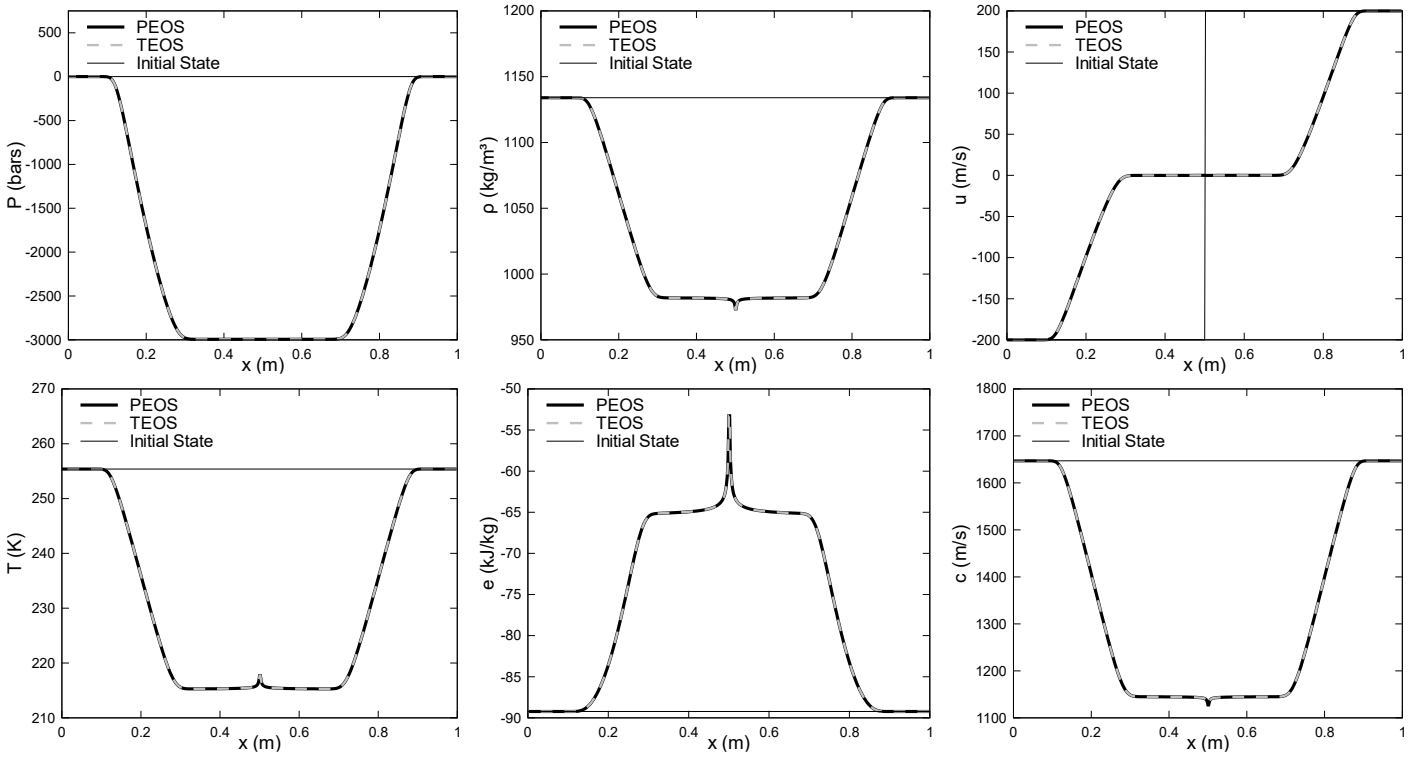

Figure 4. Single-phase double-expansion test case at velocity ± 200 m/s for the CC EOS. Dashed gray lines represent computed results with the conventional method (TEOS), and black lines correspond to the relaxation method (PEOS). Thin black lines represent the initial conditions. Results are shown at time 200 μs. Again, the results for both methods are merged. The present relaxation method perfectly recovers the TEOS results.

The conclusion is the same as for the shock-tube tests, the results are merged with both methods. The oscillation in the middle of the domain is called *overheating*, which is a numerical artifact due to the conservative formulation of the Euler equations. See for instance Toro (1995), Cocchi et al. (1998) for more details. This artefact is present in all double-expansion tests and has no serious consequences for the present illustrations.

The next test is identical except that the initial velocity is superior: ± 331 m/s. In this case, the conventional method fails at a certain point because a negative square sound speed appears. The relaxation method runs until the end. The results are shown in Figure 5. Each curve shows the solution every 50 μs and the final time is 200 μs.

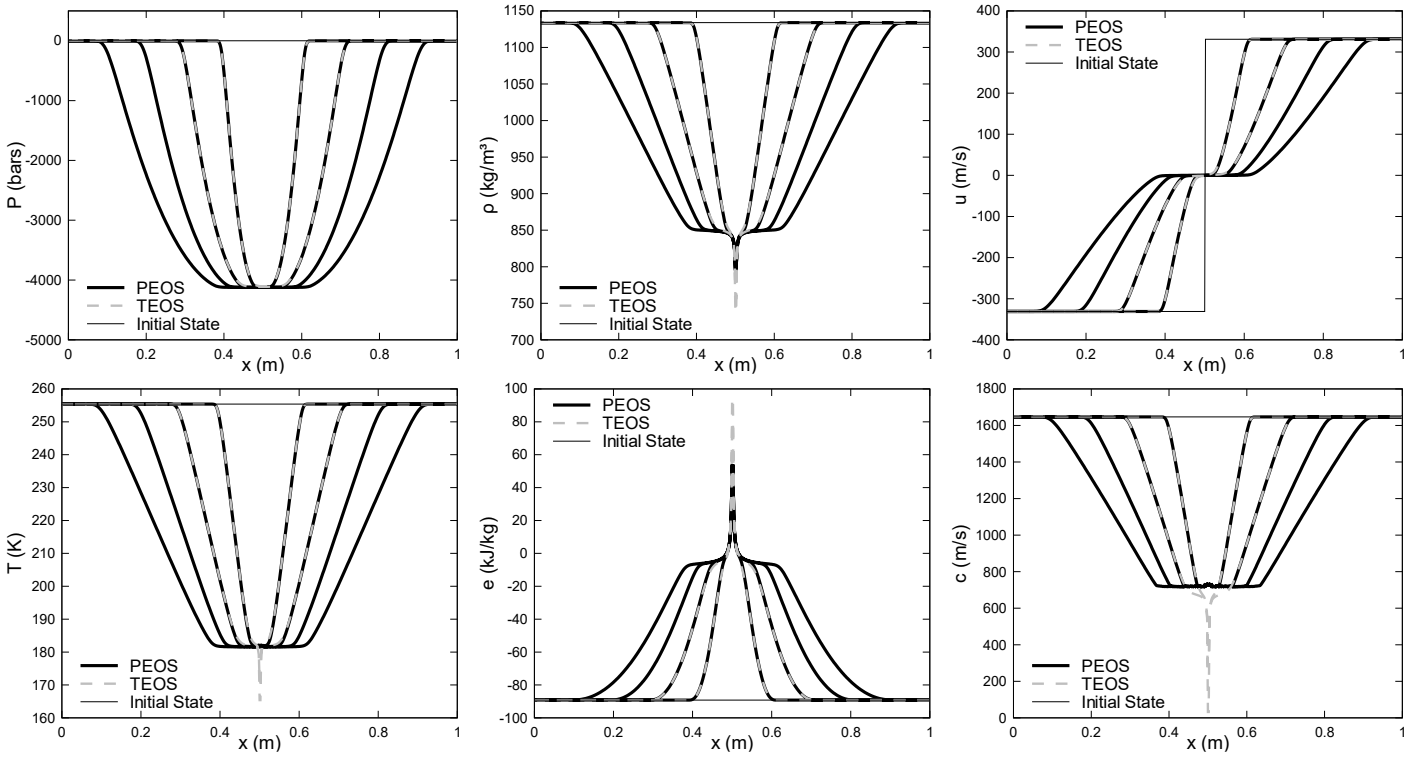

Figure 5. Single-phase double-expansion test case at velocity ± 331 m/s for the CC EOS. Dashed gray lines represent computed results with the conventional method (TEOS), and black lines correspond to the relaxation method (PEOS). Thin black lines represent the initial conditions. Each curve shows computed results every 50 μs until 200 μs. The conventional method fails after time 100 μs while the relaxation method runs until the end. In the middle of the domain, the MG convexity criteria are violated. Consequently, the PEOS parameters are not reset, preventing computational failure.

In this test case, the conventional method with CC EOS fails between times 100 μs and 150 μs because the square sound speed becomes negative in the center of the domain. The first two curves in each graph show that the two methods are identical at the beginning of the computation. Then, when sound speed goes below 800 m/s, which corresponds approximately to a density of 900 kg/m^3, the predictions between the two methods diverge. This corresponds to the moment when the convexity criteria (4.15) are no longer satisfied. Consequently, the thermodynamic parameters of the predictor EOS are no longer relaxed. As time evolves, the PEOS gradually deviates from the target EOS. The deviations here are mainly visible in the sound speed. When the conventional method fails, the new method with relaxation turned off continues, with computed results in correct agreement with those obtained at earlier times. As the solution is self-similar, it shows that the switched-off relaxation is accurate. Indeed, plateau values at the end of expansion waves are correctly computed.

A similar double-expansion test is conducted with the JWL formulation. The domain is initially set at $P = 1$ bar and $\rho = 500\ \mathrm{kg/m^3}$ with an expansion velocity of ± 261 m/s. The results are shown in Figure 6. Each curve corresponds to the solution every 100 μs and the final time is 400 μs.

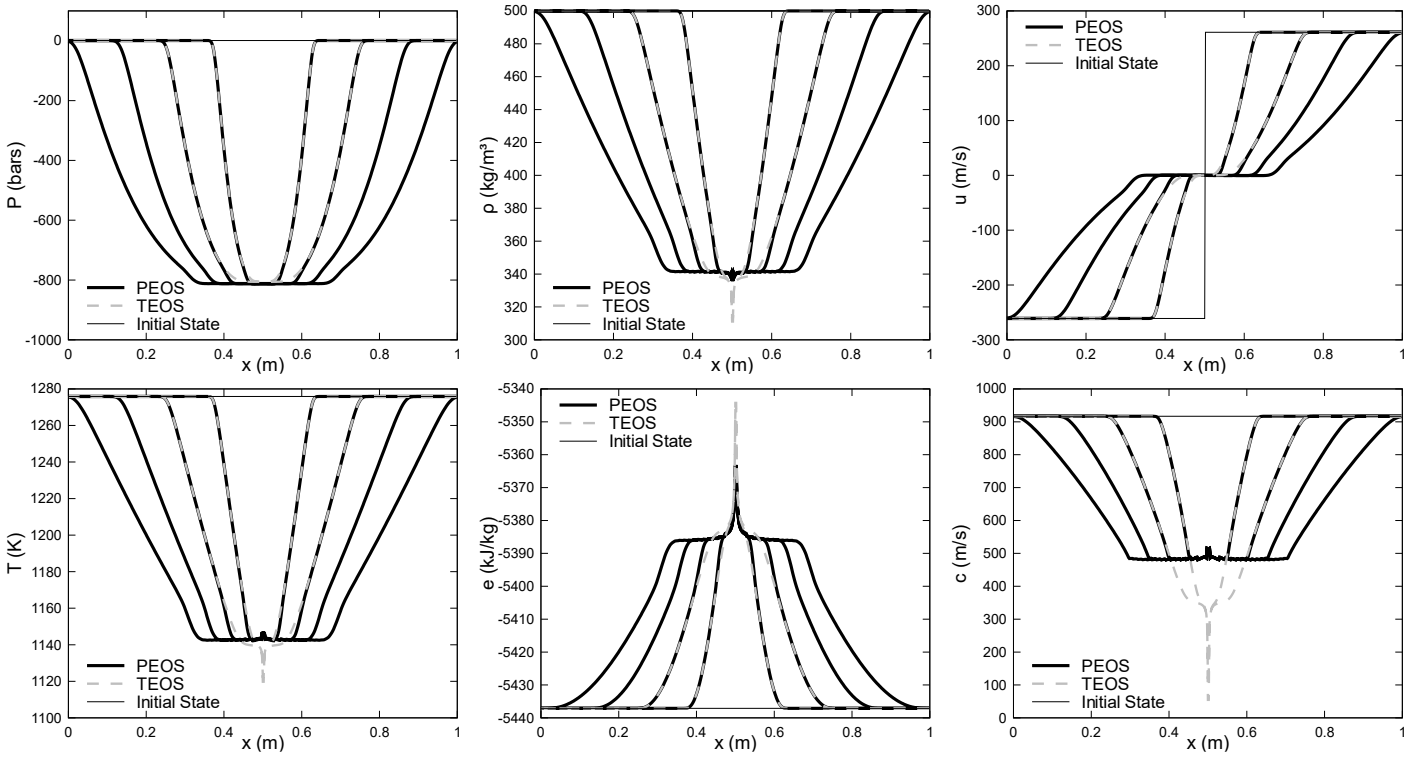

Figure 6. Single-phase double-expansion test case at velocity ± 261 m/s with the JWL EOS. Dashed gray lines represent computed results with the conventional method (TEOS), and black lines correspond to the relaxation method (PEOS). Thin black lines represent the initial conditions. Each curve corresponds to results every 100 µs until 400 µs. The conventional method fails while the relaxation method runs until the end. In the middle of the domain, the MG convexity criteria are not fulfilled. Consequently, the PEOS parameters are not reset, preventing computational failure.

The conventional method fails between times 200 µs and 300 µs, again because the square sound speed becomes negative in the middle of the domain. Overall, the conclusions are similar to the previous test case with CC. Below 360 kg/m^3, the convexity criteria are no longer met, and the relaxation step is bypassed. This allows the predictor EOS to complete the computation.

It is worth mentioning that these computational initial data are particularly severe for the JWL EOS. Indeed, this EOS models the thermodynamics of a gas phase. But because of the expansion process, the pressure becomes negative. This is obviously not physical for a gas. But it can happen with the JWL formulation as it was fitted in a restricted domain of thermodynamic conditions. And such an anomaly can also occur in multiphase flow solvers, when the gas phase is present in minor proportions. Therefore, the new method is helpful for such extreme thermodynamic conditions.

5.3. 1D spherical underwater explosion

In this section, a lagrangian scheme is used to compute an underwater explosion test. 1D lagrangian schemes enable straightforward computation of material interfaces separating two pure media. Only a single fluid is present within each computational cell, and mixture cells are prevented. The solution is updated using the following 1D numerical scheme,

$$U_i^{n+1} = \frac{1}{\Delta x_i^{n+1}}\left[\Delta x_i^n U_i^n - \Delta t\left(F_{i+1/2}^{lag,*} - F_{i-1/2}^{lag,*}\right)\right],$$

$$\text{with} \quad U = \begin{pmatrix} \rho \\ \rho u \\ \rho E \end{pmatrix} \quad \text{and} \quad F^{lag,*} = \begin{pmatrix} 0 \\ P^* \\ u^* \end{pmatrix}. \tag{5.1}$$

In Relation (5.1), indexes i and $i \pm 1/2$ denote the center of the numerical cell i and its corresponding boundaries respectively. The space step for the numerical cell i is $\Delta x_i = x_{i+1/2} - x_{i-1/2}$ and the time step is Δt. Indexes n and $n+1$ denote two consecutive time steps. The positions of the numerical cell boundaries are updated as $x_{i\pm1/2}^{n+1} = x_{i\pm1/2}^n + u_{i\pm1/2}^* \Delta t$. In this work, the intercell pressure P^* and velocity u^* are computed using the HLL (Harten, Lax, and van Leer, 1983) approximation and the wave speed estimates of Davis (1988). Further details about lagrangian methods may be found in Maire and Nkonga (2009).

A 1D spherical underwater explosion is examined in this section. A sphere containing PBXN-109 detonation products is initially settled in water. The initial radius of the sphere is 11.3 cm. The PBXN-109 detonation products are described by the JWL EOS. The thermodynamic relaxation method does not pose any particular difficulty in the lagrangian framework and follows the same lines as introduced in Section 4 for the Euler formulation. The JWL equation of state is of MG type, so there are no covolume effects and only three coefficients, R^*, P_∞^*, and q^*, are necessary for the thermodynamic relaxation method. Liquid water is described by the NASG EOS that reduces to the stiffened-gas (SG) EOS. The various EOS parameters are reported in Table II.

SG parameters (liquid water)		**JWL parameters (PBXN-109 detonation products)**	
$R\ (J/kg/K)$	2603.34	Γ	0.226
$C_v\ (J/kg/K)$	1607	$C_v\ (J/kg/K)$	1960
$P_\infty\ (Pa)$	9058×10^5	$A\ (GPa)$	1235.851
$q\ (J/kg)$	-1.15×10^6	$B\ (GPa)$	18.289
		$C\ (GPa)$	1.76
		R_1	6.104
		R_2	1.434
		$\rho_{ref}\ (kg/m^3)$	1662.039
		$D_{CJ}\ (m/s)$	7108.23
		$P_{CJ}\ (GPa)$	19.842
		$T_{CJ}\ (K)$	4824.79

Table II. Stiffened-gas (SG) and Jones-Wilkins-Lee (JWL) parameters for the 1D spherical underwater explosion test with a lagrangian scheme.

The domain is 40-cm long and is spatially resolved with 1000 cells. The PBXN-109 detonation products are initially set at $P = 7$ GPa and $\rho = 1662.039\ kg/m^3$. The liquid water is initially set at $P = 1$ bar and $\rho = 1000\ kg/m^3$. The conventional method fails as a negative square sound speed

arises. Conversely, the relaxation method completes the computation. The results are shown in Figure 7, displaying a curve for each solution at 25 μs intervals with a final time of 100 μs.

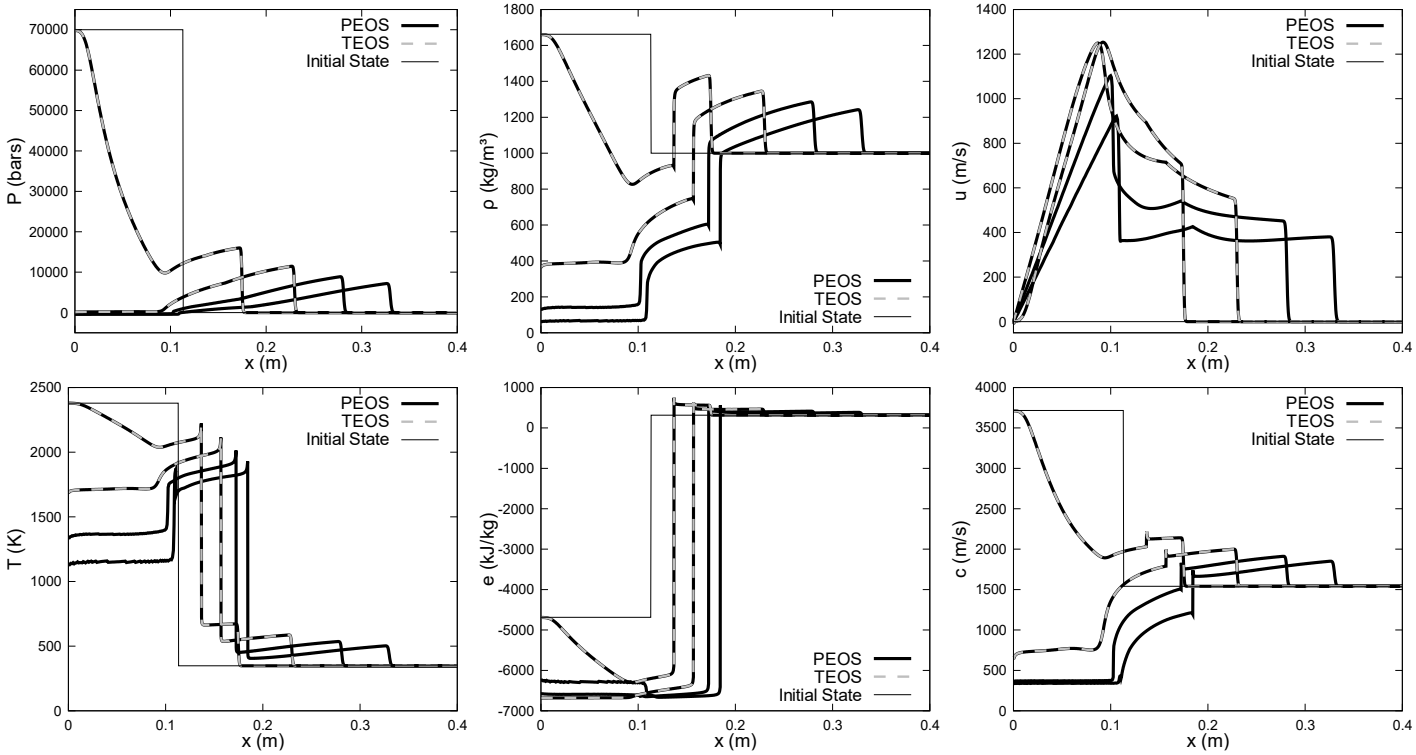

Figure 7. 1D spherical underwater explosion test with a lagrangian Godunov scheme. Dashed gray lines represent computed results with the conventional method (TEOS), and black lines correspond to the relaxation method (PEOS). Thin black lines represent the initial conditions. Each curve shows computed results every 25 μs until 100 μs. The conventional method fails after time 50 μs while the relaxation method runs until the end. At the center of the detonation-product bubble, the conventional method violates the convexity criteria of the JWL EOS. Conversely, the relaxation method does not reset the PEOS parameters, which prevents computational failure.

The conventional method fails between 50 μs and 75 μs because the square sound speed of the detonation products becomes negative at the center of the detonation-product bubble. Expansion effects lead the detonation products to vacuum conditions resulting in negative square sound speed. The first two curves in each graph show that the results computed using the conventional method (TEOS) and the thermodynamic relaxation method (PEOS) are merged during the early stages of the computation. At a certain point, the convexity criteria (4.15) are no longer satisfied, and the relaxation method bypasses the reset step (4.8), preventing computational failure.

In terms of computational time, both methods are nearly identical. No computational gain was expected in single-phase computations. As mentioned in the Introduction, CPU (Central Processing Unit) time restrictions occur in multiphase flows where relaxation solvers are mandatory. More specifically, pressure relaxation requires the solution of two interleaved Newton procedures when a phase governed by the MG EOS is present, which increases the computational time. This difficulty is alleviated with the relaxation method when the NASG EOS is used instead. In the following sections, the present thermodynamic relaxation method is investigated in various multiphase flow formulations.

6. Extension to multiphase flow models

6.1. Baer and Nunziato type flow model

The model of Baer and Nunziato (1986) considers a two-phase mixture evolving in total disequilibrium. The balance equations for phases l and $\tilde{l}$ are,

$$\begin{cases} \dfrac{\partial \alpha_l}{\partial t} + u_{\mathbf{I}} \dfrac{\partial \alpha_l}{\partial x} = \mu\left(P_l - P_{\tilde{l}}\right), \\ \dfrac{\partial \alpha_l \rho_l}{\partial t} + \dfrac{\partial \alpha_l \rho_l u_l}{\partial x} = 0, \\ \dfrac{\partial \alpha_l \rho_l u_l}{\partial t} + \dfrac{\partial \alpha_l \left(\rho_l u_l^2 + P_l\right)}{\partial x} = P_{\mathbf{I}} \dfrac{\partial \alpha_l}{\partial x} + \lambda\left(u_l - u_{\tilde{l}}\right), \\ \dfrac{\partial \alpha_l \rho_l E_l}{\partial t} + \dfrac{\partial \alpha_l \left(\rho_l E_l + P_l\right) u_l}{\partial x} = P_{\mathbf{I}} u_{\mathbf{I}} \dfrac{\partial \alpha_l}{\partial x} - \mu P'_{\mathbf{I}} \left(P_l - P_{\tilde{l}}\right) + \lambda u'_{\mathbf{I}} \left(u_l - u_{\tilde{l}}\right). \end{cases} \tag{6.1}$$

The notations are the same as before. In addition, the volume fraction α_l of phase l is introduced. Index l denotes the conjugate phase to $\tilde{l}$,*i.e.*, $l = 1$ implies $\tilde{l} = 2$ and vice versa. The mixture internal energy is defined as $e = \sum Y_l e_l$ where $Y_l = \alpha_l \rho_l / \rho$ denotes the mass fraction of phase l. The mixture density and pressure are defined as $\rho = \sum \alpha_l \rho_l$ and $P = \sum \alpha_l P_l$.

System (6.1) is a two-phase model for mixture flows evolving in pressure, velocity, and temperature disequilibria. The choice of interfacial average velocities $u_{\mathbf{I}}$ and pressures $P_{\mathbf{I}}$ was originally expressed with the relations $u_{\mathbf{I}} = u_2$ and $P_{\mathbf{I}} = P_1$, the symmetric choice $u_{\mathbf{I}} = u_1$ and $P_{\mathbf{I}} = P_2$ being possible as well. Saurel et al. (2003) proposed more general and symmetric estimates,

$$\begin{aligned} u_{\mathbf{I}} &= u'_{\mathbf{I}} + \text{sign}\left(\frac{\partial \alpha_1}{\partial x}\right) \frac{P_2 - P_1}{Z_1 + Z_2}, \qquad \text{with} \quad u'_{\mathbf{I}} = \frac{Z_1 u_1 + Z_2 u_2}{Z_1 + Z_2}, \\ P_{\mathbf{I}} &= P'_{\mathbf{I}} + \text{sign}\left(\frac{\partial \alpha_1}{\partial x}\right) \frac{Z_1 Z_2 \left(u_2 - u_1\right)}{Z_1 + Z_2}, \quad \text{with} \quad P'_{\mathbf{I}} = \frac{Z_1 P_2 + Z_2 P_1}{Z_1 + Z_2}, \end{aligned} \tag{6.2}$$

where $Z_l = \rho_l c_l$ represents the acoustic impedance, and c_l is the speed of sound of fluid l.

The first equation of System (6.1) is non-conservative and represents the transport of the volume fraction α_l at the interfacial velocity $u_{\mathbf{I}}$. During the advection stage, volume variations caused by pressure differences between the phases appear through the relaxation term $\mu\left(P_l - P_{\tilde{l}}\right)$ with μ controlling the rate at which pressure equilibrium is reached. The second equation of System (6.1) describes the mass balance of the corresponding phase while the third equation is related to its momentum balance. This relation is non-conservative. The velocity relaxation term on the right-hand side of the momentum equations reads $\lambda\left(u_l - u_{\tilde{l}}\right)$ where λ is the product of the specific interfacial area with the drag coefficient. It controls the rate at which the velocities tend toward equilibrium. Finally, the fourth equation of System (6.1) describes the energy balance of phase l. This latter is also non-conservative due to the presence of the term $P_{\mathbf{I}} u_{\mathbf{I}} \dfrac{\partial \alpha_l}{\partial x}$ and the relaxation terms on the right-hand side.

System (6.1) is hyperbolic with wave speeds u_I, u_l, and $u_l \pm c_l$, , thermodynamically consistent and symmetric. Its extension to more than two phases is possible (see Chinnayya et al., 2004 for instance). In the frame of the present contribution, System (6.1) is augmented by three transport-relaxation equations for each phase l, written under a conservative form with the help of the corresponding mass relation (in the absence of mass transfer),

$$\begin{cases} \dfrac{\partial \alpha_l \rho_l P^*_{\infty,l}}{\partial t} + \dfrac{\partial \alpha_l \rho_l P^*_{\infty,l} u_l}{\partial x} = \dfrac{\alpha_l \rho_l}{\tau}\left(P_{\infty,l}\left(v_l\right) - P^*_{\infty,l}\right), \\ \dfrac{\partial \alpha_l \rho_l R^*_l}{\partial t} + \dfrac{\partial \alpha_l \rho_l R^*_l u_l}{\partial x} = \dfrac{\alpha_l \rho_l}{\tau}\left(R_l\left(v_l, e_l\right) - R^*_l\right), \\ \dfrac{\partial \alpha_l \rho_l q^*_l}{\partial t} + \dfrac{\partial \alpha_l \rho_l q^*_l u_l}{\partial x} = \dfrac{\alpha_l \rho_l}{\tau}\left(q_l\left(v_l\right) - q^*_l\right), \\ \text{with } \tau \to 0^+ \text{ when the convexity relations (4.15) are fulfilled, otherwise } \tau \to +\infty. \end{cases} \tag{6.3}$$

System (6.1) includes pressure and velocity relaxation source terms. Relaxation phenomena are then addressed depending on the flow conditions. Those relaxation processes may yield total or partial equilibrium depending on the rate at which the corresponding equilibrium is supposed to be reached. For example, in the context of deflagration-to-detonation transition in a granular explosive, typical timescales associated with the pressure and velocity relaxation processes are small (Kapila et al. 2001). Stiff pressure and velocity solvers are consequently used. Details can be found for example in Le Métayer et al. (2013).

Stiff velocity relaxation solver does not involve thermodynamics. However, the computation of the instantaneous pressure equilibrium involves the equations of state of the fluids. An example of a stiff pressure relaxation solver is recalled hereafter and adapted to the present TEOS and PEOS. Following the various relaxations processes, the present thermodynamic relaxation step (4.8) is achieved if the convexity criteria (4.15) are met. Otherwise, thermodynamic relaxation is bypassed, as detailed in Section 4.4.

6.2. Stiff pressure relaxation

The phases as described by System (6.1) are initially in pressure disequilibrium. At the end of the pressure relaxation process, the phases have a common pressure, the other variables (velocity, temperature) being potentially different. In the presence of the pressure relaxation terms only, the ordinary-differential-equation system to examine for each phase l reads,

$$\begin{cases} \dfrac{\partial \alpha_l}{\partial t} = \mu\left(P_l - P_{\tilde{l}}\right), \\ \dfrac{\partial \alpha_l \rho_l}{\partial t} = 0, \\ \dfrac{\partial \alpha_l \rho_l u_l}{\partial t} = 0, \\ \dfrac{\partial \alpha_l \rho_l E_l}{\partial t} = -\mu P'_I \left(P_l - P_{\tilde{l}}\right). \end{cases} \tag{6.4}$$

As instantaneous pressure relaxation is addressed, there is no need for a precise knowledge of the pressure relaxation parameter μ that is considered very large $\mu \to +\infty$. The second (mass) and third (momentum) equations of System (6.4) indicate that the velocity u_l remains unchanged during the

pressure relaxation process. Consequently, a stiff velocity relaxation solver may be used beforehand, the relaxed velocity is not affected.

The second relation of System (6.4) involves mass conservation for each phase during the pressure relaxation process:

$$\alpha_l^{(0)}\rho_l^{(0)} = \alpha_l^{(1)}\rho_l^{(1)}, \tag{6.5}$$

where superscripts "(0)" and "(1)" denote the initial (post-hyperbolic) and final (relaxed) states respectively. In addition, with the help of velocity invariance, the combination of the first and fourth equations of (6.4) yields

$$e_l^{(1)} = e_l^{(0)} - P^{(1)}\left(v_l^{(1)} - v_l^{(0)}\right), \tag{6.6}$$

where $P_I' = \text{const} = P^{(1)}$ (common pressure to all phases) has been considered. The EOSs of the various phases are necessary to express the relaxed specific internal energy $e_l^{(1)}$ in (6.6) as a function of the relaxed specific volume $v_l^{(1)}$ and relaxed pressure $P^{(1)}$. The sought relaxed pressure is then computed through the fulfillment of the saturation constraint $\left(\sum \alpha_l^{(0)} = \sum \alpha_l^{(1)} = 1\right)$ written below with the help of (6.5) as,

$$\sum\left(\alpha_l^{(0)}\rho_l^{(0)}v_l^{(1)}\right) - 1 = 0. \tag{6.7}$$

The target EOS and predicted EOS are addressed hereafter. The goal is to showcase the simplicity and efficiency resulting from the present thermodynamic relaxation method. Indeed, with the TEOS, pressure relaxation requires two imbricated Newton loops, while a single procedure is needed with PEOS.

a) Target EOS (TEOS)

In the present context, TEOS is of MG form. The caloric formulation of the MG EOS (2.1) expresses as,

$$e_l^{(1)}\left(P_l^{(1)}, v_l^{(1)}\right) = \frac{\left(P_l^{(1)} - P_{l,k}\left(v_l^{(1)}\right)\right)v_l^{(1)}}{\Gamma_l} + e_{l,k}\left(v_l^{(1)}\right). \tag{6.8}$$

The combination of Relations (6.6) and (6.8) yields the following function,

$$g\left(P^{(1)}, v_l^{(1)}\right) = \frac{\left(P_l^{(1)} - P_{l,k}\left(v_l^{(1)}\right)\right)v_l^{(1)}}{\Gamma_l} + e_{l,k}\left(v_l^{(1)}\right) - e_l^{(0)} + P^{(1)}\left(v_l^{(1)} - v_l^{(0)}\right) = 0. \tag{6.9}$$

The specific volume in the final state $v_l^{(1)}$ then depends on the pressure $P^{(1)}$. The saturation constraint (6.7) consequently becomes a function of the relaxed pressure $P^{(1)}$,

$$f\left(P^{(1)}\right) = \sum\left(\alpha_l^{(0)}\rho_l^{(0)}v_l^{(1)}\left(P^{(1)}\right)\right) - 1 = 0. \tag{6.10}$$

The resolution of Relation (6.10) provides the pressure in the final state $P^{(1)}$, common to all phases. An iterative method, such as the algorithm of Newton, is necessary. However, the expression of the specific volume $v_l^{(1)}$ is not explicit with (6.9) for the general MG EOS due to the dependence of the

$\mathrm{P}_{l,\mathrm{k}}\left(\mathrm{v}_l^{(1)}\right)$ and $\mathrm{e}_{l,\mathrm{k}}\left(\mathrm{v}_l^{(1)}\right)$ terms on the specific volume. Consequently, for a given pressure $\mathrm{P}^{(1)}$ of the iterative procedure, another iterative method is needed to compute $\mathrm{v}_l^{(1)}\left(\mathrm{P}^{(1)}\right)$, satisfying Relation (6.9). Two imbricated Newton loops are then necessary when a phase governed by the MG EOS is considered, increasing consequently computational time.

b) Predictor EOS (PEOS)

The PEOS is of NASG-type so the expression of the specific volume is explicit. The caloric formulation of the NASG EOS (3.1) expresses as,

$$\mathrm{e}_l^{(1)}\left(\mathrm{P}_l^{(1)},\mathrm{v}_l^{(1)}\right)=\left(\frac{\mathrm{C}_{\mathrm{v},l}^*}{\mathrm{R}_l^*}\left(\mathrm{P}_l^{(1)}+\mathrm{P}_{\infty,l}^*\right)+\mathrm{P}_{\infty,l}^*\right)\left(\mathrm{v}_l^{(1)}-\mathrm{b}_l^*\right)+\mathrm{q}_l^*. \tag{6.11}$$

The combination of Relations (6.6) and (6.11) then yields an explicit formulation of the relaxed specific volume,

$$\mathrm{v}_l^{(1)}\left(\mathrm{P}^{(1)}\right)=\frac{\mathrm{C}_{\mathrm{v},l}^*\mathrm{v}_l^{(0)}}{\mathrm{C}_{\mathrm{v},l}^*+\mathrm{R}_l^*}\left(\frac{\mathrm{R}_l^*}{\mathrm{C}_{\mathrm{v},l}^*}+\frac{\mathrm{P}_l^{(0)}+\mathrm{P}_{\infty,l}^*}{\mathrm{P}^{(1)}+\mathrm{P}_{\infty,l}^*}\right)-\frac{\mathrm{C}_{\mathrm{v},l}^*\mathrm{b}_l^*\left(\mathrm{P}_l^{(0)}-\mathrm{P}^{(1)}\right)}{\left(\mathrm{C}_{\mathrm{v},l}^*+\mathrm{R}_l^*\right)\left(\mathrm{P}^{(1)}+\mathrm{P}_{\infty,l}^*\right)}. \tag{6.12}$$

Consequently, a single iterative method is necessary to compute the pressure $\mathrm{P}^{(1)}$, solution to the saturation constraint (6.7), reformulated hereafter as,

$$\mathrm{f}\left(\mathrm{P}^{(1)}\right)=\sum\left(\alpha_l^{(0)}\rho_l^{(0)}\mathrm{v}_l^{(1)}\left(\mathrm{P}^{(1)}\right)\right)-1=0. \tag{6.13}$$

As (6.12) is explicit, a single Newton loop is needed to solve (6.13). Furthermore, in the specific case where only two phases are present, an explicit solution appears. Indeed, after some algebraic manipulations, the combination of (6.12) and (6.13) leads to,

$$\begin{aligned}\mathrm{P}^{(1)}=&\frac{\mathrm{A}_1+\mathrm{A}_2-\left(\mathrm{P}_{\infty,1}^*+\mathrm{P}_{\infty,2}^*\right)-\mathrm{B}_1\left(\mathrm{P}_1^{(0)}-\mathrm{P}_{\infty,2}^*\right)-\mathrm{B}_2\left(\mathrm{P}_2^{(0)}-\mathrm{P}_{\infty,1}^*\right)}{2\left(1-\mathrm{B}_1-\mathrm{B}_2\right)}\\&+\frac{1}{\left(1-\mathrm{B}_1-\mathrm{B}_2\right)}\sqrt{\frac{1}{4}\left(\mathrm{A}_2-\mathrm{A}_1-\left(\mathrm{P}_{\infty,2}^*-\mathrm{P}_{\infty,1}^*\right)\right)^2+\mathrm{A}_1\mathrm{A}_2+\frac{\mathrm{C}}{4}},\end{aligned} \tag{6.14}$$

with,

$$\mathrm{A}_1=\frac{\dfrac{\mathrm{C}_{\mathrm{v},1}^*\alpha_1^{(0)}}{\mathrm{C}_{\mathrm{v},1}^*+\mathrm{R}_1^*}\left(\mathrm{P}_1^{(0)}+\mathrm{P}_{\infty,1}^*\right)}{\dfrac{\mathrm{C}_{\mathrm{v},1}^*\alpha_1^{(0)}}{\mathrm{C}_{\mathrm{v},1}^*+\mathrm{R}_1^*}+\dfrac{\alpha_2^{(0)}}{\mathrm{C}_{\mathrm{v},2}^*+\mathrm{R}_2^*}},\quad \mathrm{A}_2=\frac{\dfrac{\mathrm{C}_{\mathrm{v},2}^*\alpha_2^{(0)}}{\mathrm{C}_{\mathrm{v},2}^*+\mathrm{R}_2^*}\left(\mathrm{P}_2^{(0)}+\mathrm{P}_{\infty,2}^*\right)}{\dfrac{\mathrm{C}_{\mathrm{v},1}^*\alpha_1^{(0)}}{\mathrm{C}_{\mathrm{v},1}^*+\mathrm{R}_1^*}+\dfrac{\mathrm{C}_{\mathrm{v},2}^*\alpha_2^{(0)}}{\mathrm{C}_{\mathrm{v},2}^*+\mathrm{R}_2^*}}, \tag{6.15}$$

$$\mathrm{B}_1=\frac{\dfrac{\mathrm{C}_{\mathrm{v},1}^*\alpha_1^{(0)}}{\mathrm{C}_{\mathrm{v},1}^*+\mathrm{R}_1^*}\dfrac{\mathrm{b}_1^*}{\mathrm{v}_1^{(0)}}}{\dfrac{\mathrm{C}_{\mathrm{v},1}^*\alpha_1^{(0)}}{\mathrm{C}_{\mathrm{v},1}^*+\mathrm{R}_1^*}+\dfrac{\mathrm{C}_{\mathrm{v},2}^*\alpha_2^{(0)}}{\mathrm{C}_{\mathrm{v},2}^*+\mathrm{R}_2^*}},\quad \mathrm{B}_2=\frac{\dfrac{\mathrm{C}_{\mathrm{v},2}^*\alpha_2^{(0)}}{\mathrm{C}_{\mathrm{v},2}^*+\mathrm{R}_2^*}\dfrac{\mathrm{b}_2^*}{\mathrm{v}_2^{(0)}}}{\dfrac{\mathrm{C}_{\mathrm{v},1}^*\alpha_1^{(0)}}{\mathrm{C}_{\mathrm{v},1}^*+\mathrm{R}_1^*}+\dfrac{\mathrm{C}_{\mathrm{v},2}^*\alpha_2^{(0)}}{\mathrm{C}_{\mathrm{v},2}^*+\mathrm{R}_2^*}}, \tag{6.16}$$

$$\begin{aligned}\mathrm{C}=&\left(\mathrm{B}_1\left(\mathrm{P}_1^{(0)}-\mathrm{P}_{\infty,2}^*\right)+\mathrm{B}_2\left(\mathrm{P}_2^{(0)}-\mathrm{P}_{\infty,1}^*\right)\right)^2+2\left(\mathrm{P}_{\infty,1}+\mathrm{P}_{\infty,2}-\mathrm{A}_1-\mathrm{A}_2\right)\left(\mathrm{B}_1\left(\mathrm{P}_1^{(0)}-\mathrm{P}_{\infty,2}^*\right)+\mathrm{B}_2\left(\mathrm{P}_2^{(0)}-\mathrm{P}_{\infty,1}^*\right)\right)\\&-4\left(1-\mathrm{B}_1-\mathrm{B}_2\right)\left(\mathrm{B}_1\mathrm{P}_1^{(0)}\mathrm{P}_{\infty,2}^*+\mathrm{B}_2\mathrm{P}_2^{(0)}\mathrm{P}_{\infty,1}^*\right)-4\left(\mathrm{B}_1+\mathrm{B}_2\right)\left(\mathrm{A}_1\mathrm{P}_{\infty,2}^*+\mathrm{A}_2\mathrm{P}_{\infty,1}^*-\mathrm{P}_{\infty,1}^*\mathrm{P}_{\infty,2}^*\right).\end{aligned} \tag{6.17}$$

6.3. Multiphase 1D results

The flow model (6.1) can be used for a wide range of applications:

- Two-phase mixtures evolving in velocity and temperature disequilibria, such as bubbly flows and dispersed flows with droplets or solid particles in a gas.
- Interfacial flows, present when two materials are separated by an interface. In this frame two options are possible.
    - The use of stiff pressure and velocity relaxation solvers enables the flow model to fulfill the interface conditions. It was done in Saurel and Abgrall (1999a). Kapila et al. (2001) derived reduced equations with a single velocity and a single pressure in the same direction.
    - The use of non-conservative terms. These terms can match the interface conditions of equal velocities and pressures when the volume fraction is discontinuous and varies between 0 and 1. This feature is also useful for permeable interfaces, when the volume fraction is continuous or varies between a more restricted range. Examples can be found in Saurel et al. (2014). However, this option requires accurate (even exact) computation of the non-conservative terms, meaning that local interfacial pressure and velocity, computed with an Euler-Euler Riemann solver is needed. In many applications, when the material EOSs are complicated, accurate computation of these interfacial variables is challenging because exact Riemann solvers for such EOSs are too expensive in terms of computation time. The use of approximate Riemann solvers, such as HLLC, is challenging as the wave speed estimate is problematic when contact waves separate two fluids having very different sound speeds.

In this section, the present relaxation method is illustrated for the computation of interfacial flows, first with pressure and velocity relaxation solvers, and second with non-conservative terms. This last option is the most challenging regarding robustness and accuracy with respect to the computation of the non-conservative terms.

The numerical scheme used to solve System (6.1)-(6.2), and (6.3) is the Discrete Equations Method (DEM) from Abgrall and Saurel (2003). In the DEM, Riemann solvers for the Euler equations only are used. With the present thermodynamic relaxation method, the various Riemann problem computations, with the corresponding contacts 1-1, 1-2, 2-1, and 2-2, are done using exact Riemann solvers. This is possible because the PEOS is the stiffened-gas equation of state (the covolume is set to $b_l^* = 0$). An appropriate exact Riemann solver is given for example in Godunov et al. (1976).

Note that the same computations may be done with the method of Furfaro and Saurel (2015). In this framework, the present thermodynamic relaxation method is used to compute the lagrangian fluxes in order to improve computational accuracy of P_I and u_I present in both the corresponding 4-wave Riemann solver and in the non-conservative terms.

For the sake of clarity, the DEM is used with exact Riemann solver. The computations are performed with a second-order scheme in space and time on a 2000-cell grid and the results are displayed in Figure 8 when the first option is used. The time step is computed with a CFL criterion of 0.5.

The initial conditions involve a membrane located at 0.8 m separating nitromethane with a density equal to $\rho = 1134 \text{ kg/m}^3$ and governed by the CC EOS (with parameters given in Table I) from air

with a density equal to $\rho = 50\ \mathrm{kg/m^3}$ and governed by the ideal-gas EOS with a specific heat coefficient equal to $C_v = 719\ \mathrm{J.kg^{-1}.K^{-1}}$ and an adiabatic coefficient equal to $\gamma = 1.4$, resulting in $R = (\gamma - 1)C_v = 287.6\ \mathrm{J.kg^{-1}.K^{-1}}$. The left chamber is initially set at pressure $P = 2000$ bars and the right chamber is set at the atmospheric pressure $P = 1$ bar. The final time is set to 276 µs. The volume fraction of nitromethane is set to 10^{-6} in the right chamber and the volume fraction of air to 10^{-6} in the left chamber.

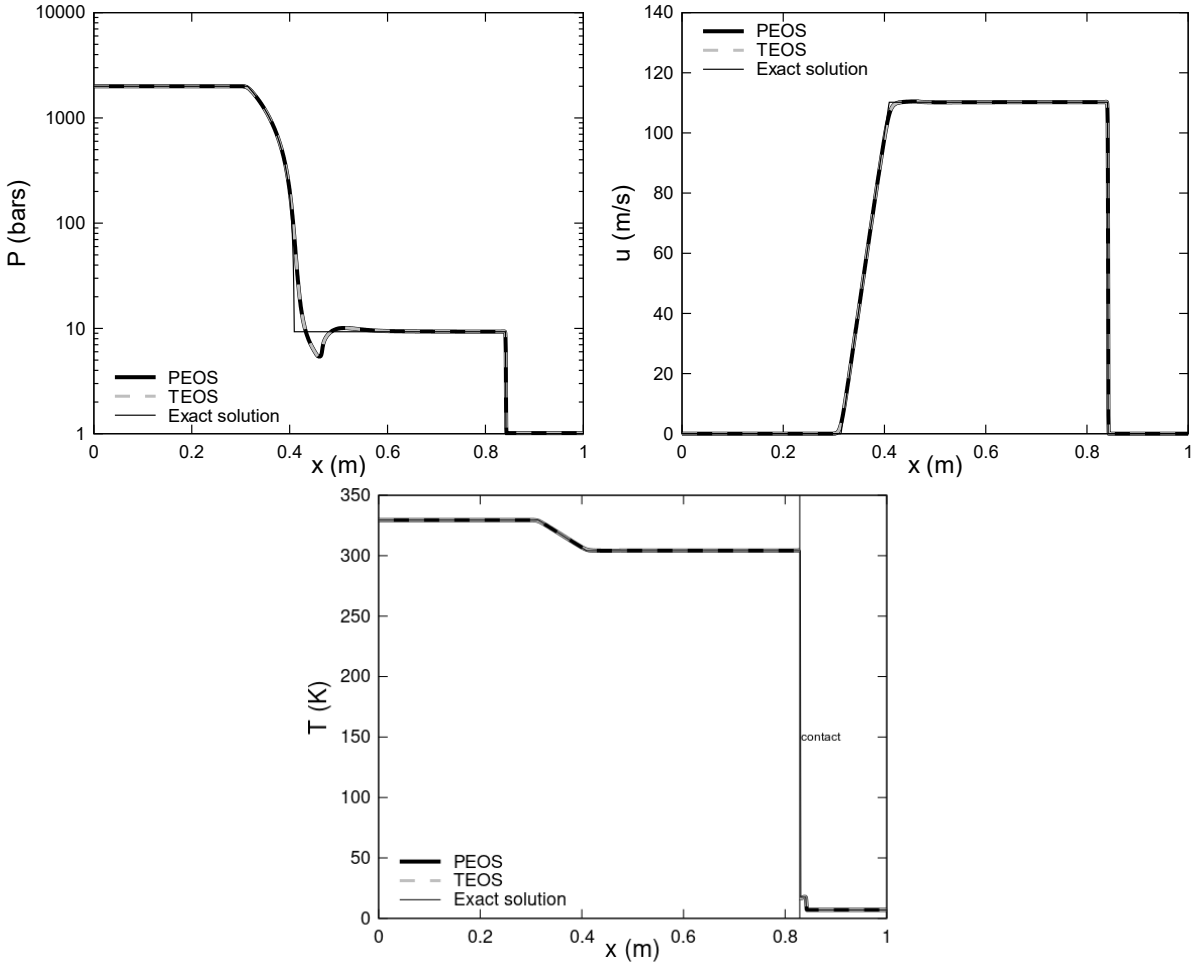

Figure 8. Shock-tube test case with the symmetric variant of the Baer and Nunziato equations with instantaneous velocity and pressure relaxations. Dashed gray lines represent computed results with the conventional method (TEOS), and black lines correspond to the relaxation method (PEOS). Thin black lines represent the exact solution computed with the Riemann solver of Saurel et al. (1994). Results are shown at time 276 µs. As pressure and velocity are instantaneously relaxed, only one pressure and one velocity are displayed. Since temperatures are in disequilibrium, the nitromethane temperature is shown on the left of the contact, while the air temperature is displayed on the right. The present relaxation method perfectly recovers the target EOS results.

The results computed with the relaxation method using PEOS are merged with those obtained with the conventional method using TEOS. Furthermore, the use of the NASG EOS expressions throughout the numerical code is computationally cheaper than with CC EOS. Consequently, PEOS computations are 1.8 times faster than with TEOS.

The same test with the same initial conditions is now re-run without pressure and velocity relaxation solvers. In the absence of relaxation terms, each fluid evolves with its own pressure, velocity, and

temperature. Coupling between the fluids is therefore solely controlled by the non-conservative terms on the right-hand side of System (6.1) that enforce continuity of pressure and velocity across the contact wave.

This test case is quite sensitive to the discretization of the non-conservative terms. The HLLC solver used so far in the Discrete Equations Method is a versatile approximate Riemann solver that can be easily extended to complex EOSs but requires an accurate estimation of the wave speeds. Various estimates are for example given in Toro (1999). However, none of them is appropriate when material discontinuities are present. An exact Riemann solver could be used with general EOSs (Saurel et al. 1994), but it is too expensive. Using the PEOS in this context is of significant interest as it reduces to the stiffened-gas EOS. Exact Riemann solvers for the Euler equations with the stiffened-gas EOS have been derived for instance in Godunov et al., (1976), Plohr (1988).

The aim of the following test is to compare the solution obtained with the HLLC solver using TEOS with the exact solver using PEOS. The results are shown in Figure 9 (pressures) and Figure 10 (velocities).

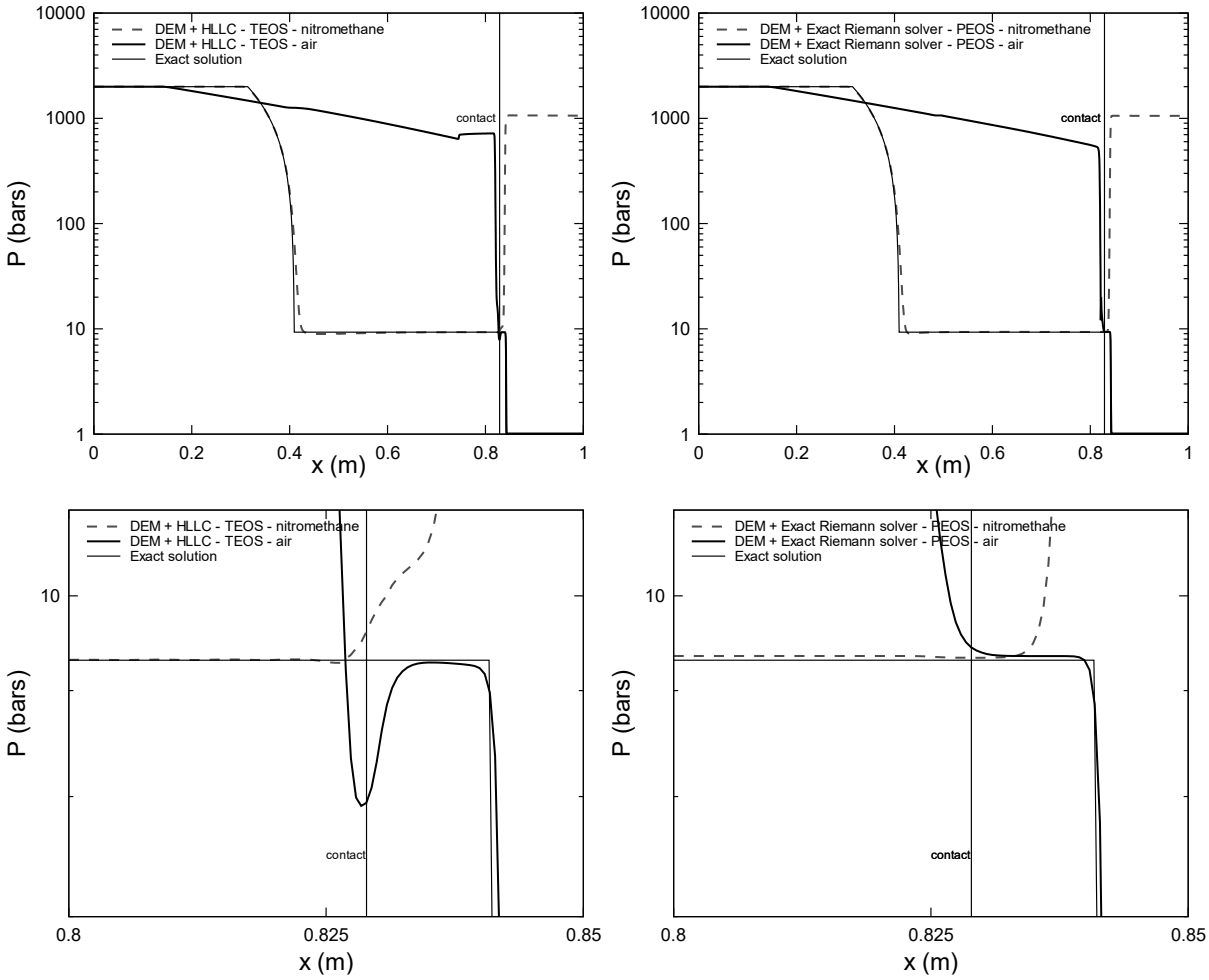

Figure 9. Shock-tube test case with the symmetric variant of the Baer and Nunziato equations in the absence of relaxation terms. In this test case, the contact conditions are fulfilled only by the action of the non-conservative terms. The left column shows the results associated with the Discrete Equations Method (DEM) and the HLLC solver, whereas the right column shows the results associated with the DEM and the exact Riemann solver for the stiffened-gas EOS. The bottom figures are magnified views of the respective simulations. Thick black lines represent air whereas dashed gray lines represent nitromethane. Thin black lines represent the exact solution computed with the method of Saurel et al. (1994) and the thin vertical line indicates the exact location of the contact. The results are shown at time 276 μs. The thermodynamic relaxation method is used together with the exact Riemann solver with the stiffened-gas EOS. The nitromethane pressure on the left is perfectly matched with the air pressure in the right column (PEOS), while an oscillation is present in the left column (TEOS).

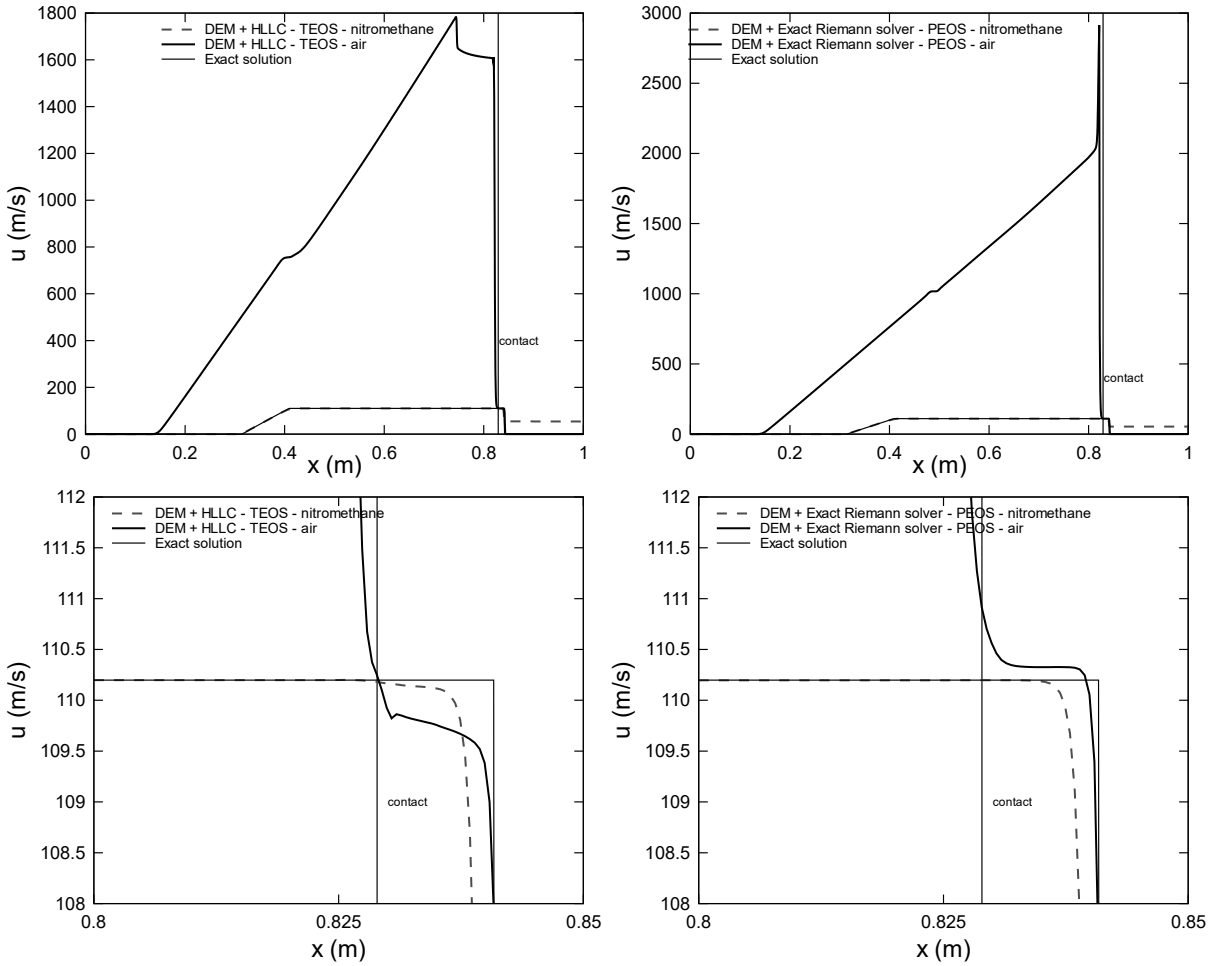

Figure 10. Same as Figure 9 but with velocities displayed instead of pressures.

With HLLC and the wave speed estimates of Davis (1988), matching is clearly perfectible resulting in a poor approximation of the gas variables to the right of the contact wave (results in the left column). On the other hand, when the exact Riemann solver based on the PEOS is used, the agreement with the exact solution is improved.

Consequently, with the present thermodynamic relaxation method, it is possible to use the Discrete Equations Method to solve the Baer-and-Nunziato-type model (6.1) with exact Riemann solvers, even when sophisticated EOSs are present. Indeed, these EOSs locally reduce to the stiffened-gas equation of state, for which an exact Riemann solver is available and suitable for computing the interface conditions through non-conservative terms.

7. Diffuse interface computations

7.1. Flow model

As mentioned earlier, one way to compute interfacial flows, is to address the Baer-and-Nunziato-type model (6.1) with stiff pressure and velocity relaxation solvers. A simpler, faster, and very robust method consists of using the homokinetic model of Saurel et al. (2009). Pressure relaxation is still present to approximate the non-conservative term of the model of Kapila et al. (2001).

The model of Saurel et al. (2009) is a hyperbolic overdetermined system composed of the following equations (presented in 1D for the sake of simplicity),

$$
\begin{cases}
\dfrac{\partial \alpha_l}{\partial t} + u \dfrac{\partial \alpha_l}{\partial x} = \mu \left(P_l - P_{\tilde{l}} \right), \ \text{with } \mu \to +\infty, \\
\dfrac{\partial \alpha_l \rho_l}{\partial t} + \dfrac{\partial \alpha_l \rho_l u}{\partial x} = 0, \\
\dfrac{\partial \rho u}{\partial t} + \dfrac{\partial \left(\rho_l u^2 + P_l \right)}{\partial x} = 0, \\
\dfrac{\partial \alpha_l \rho_l e_l}{\partial t} + \dfrac{\partial \alpha_l \rho_l e_l u}{\partial x} + \alpha_l P_l \dfrac{\partial u}{\partial x} = -\mu P_{\mathbf{I}} \left(P_l - P_{\tilde{l}} \right), \\
\dfrac{\partial \rho E}{\partial t} + \dfrac{\partial u \left(\rho E + P \right)}{\partial x} = 0.
\end{cases}
\tag{7.1}
$$

The notations remain the same as before. In addition, the mixture center of mass velocity u, common to all phases, is introduced. In the frame of the present contribution, System (7.1) is augmented by three transport-relaxation equations for each phase *l*, written under conservative form with the help of the mixture mass equation,

$$
\begin{cases}
\dfrac{\partial \rho P^*_{\infty,l}}{\partial t} + \dfrac{\partial \rho P^*_{\infty,l} u}{\partial x} = \dfrac{\rho}{\tau} \left(P_{\infty,l} \left(v_l \right) - P^*_{\infty,l} \right), \\
\dfrac{\partial \rho R^*_l}{\partial t} + \dfrac{\partial \rho R^*_l u}{\partial x} = \dfrac{\rho}{\tau} \left(R_l \left(v_l, e_l \right) - R^*_l \right), \\
\dfrac{\partial \rho q^*_l}{\partial t} + \dfrac{\partial \rho q^*_l u}{\partial x} = \dfrac{\rho}{\tau} \left(q_l \left(v_l \right) - q^*_l \right), \\
\text{with } \tau \to 0^+ \text{ when the convexity conditions } (4.15) \text{ are fulfilled, otherwise } \tau \to +\infty.
\end{cases}
\tag{7.2}
$$

The interfacial pressure appearing on the right-hand side of (7.1) reads $P_{\mathbf{I}} = \sum \left(\dfrac{P_l}{Z_l} \right) / \sum \left(\dfrac{1}{Z_l} \right)$. In this formulation, the volume fraction equation corresponds to a simple transport equation with stiff relaxation, for which there is no difficulty in preserving volume fraction positivity. The stiff pressure relaxation solver presented previously directly applies and provides the relaxed pressure $P^{(1)}$ and relaxed specific volumes $v_l^{(1)}$. In addition, following Saurel et al. (2009), the internal energies are also reset with the mixture pressure at mechanical equilibrium and the relaxed specific volumes. This task does not pose any particular difficulty for either TEOS or PEOS. The reader is then referred to the aforementioned reference. The presence of the non-conservative terms in the internal energy equations thus becomes of minor importance.

System (7.1-7.2) is hyperbolic with wave speeds u and $u \pm c_f$ with the following definition for the square sound speed: $c_f^2 = \sum Y_l c_l^2$. Numerical computations have shown excellent convergence to exact solutions for interfaces separating (nearly pure) fluids, even under extreme flow conditions. More details regarding numerical resolution of this model are available in Saurel et al. (2009), Chiapolino et al. (2017), and Saurel and Pantano (2018) for example.

7.2. Underwater explosion

A multi-dimensional illustration on an unstructured mesh is now presented. In the following, the present relaxation method is illustrated on an underwater explosion test. The computational test

corresponds to a high-pressure PBXN-109 bubble of gas products settled underwater, close to the water-air surface. Such a situation occurs when an underwater-explosion bubble reaches the surface. Relevant literature on the subject can be found for example in Holt (1977), Grove and Menikoff (1990). The detonation is not resolved but considered as a constant volume explosion resulting in high-pressure and high-density gas products. The liquid water surrounding the charge is initially considered at atmospheric conditions. The air above is at rest and at atmospheric conditions as well. The initial conditions and geometrical dimensions are depicted in Figure 11.

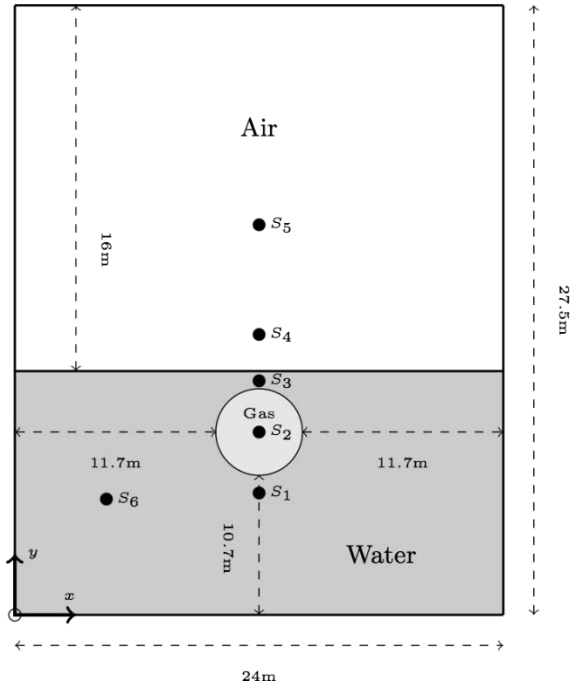

Figure 11. Initial conditions of the 2D underwater explosion test. PBXN-109 detonation products are immersed in still liquid water. Atmospheric air is present above water. Water and air are initially at 101325 Pa and 298 K. Detonation products are initially at 1 GPa and 4800 K. Maximum and minimum initial volume fractions are $\alpha_{max} = 1 - 2\times10^{-6}$ and $\alpha_{min} = 10^{-6}$. Wall boundary conditions are prescribed for all sides. Six gauge pressure and density sensors are located at coordinates $S_1 = (12, 5.75)$, $S_2 = (12, 11)$, $S_3 = (12, 11.4)$, $S_4 = (12, 13)$, $S_5 = (12, 19.5)$ and $S_6 = (6, 5.5)$.

PBXN-109 detonation products are described by the JWL EOS. Liquid water and atmospheric air are described by the NASG EOS, reducing to the stiffened-gas and ideal-gas EOSs respectively. The EOS parameters for the liquid water and PBXN-109 detonation products are given in Table II (Section 5). The EOS parameters for the air are those of Section 6.3.

The present configuration is close to the 1D underwater explosion test of Section 5.3 where computational failure of JWL has been observed. In the following computations, the heat capacity of the PBXN-109 detonation products is reduced from $C_v = 1960$ J.kg^{-1}.K^{-1} to $C_v = 1000$ J.kg^{-1}.K^{-1}. With this low value, the convexity criteria (4.15) are satisfied as shown in Appendix B. As the purpose of the present explosion test is purely illustrative, $C_v = 1000$ J.kg^{-1}.K^{-1} is adopted to enable computations with JWL. Consequently, a comparison is made between TEOS and PEOS.

The results computed with the present thermodynamic relaxation method are presented in Figure 12 in terms of mixture-pressure-gradient contours and liquid-volume-fraction contours. The mesh consists of 356,620 unstructured triangles. The hyperbolic part of System (7.1-7.2) (in the absence of source terms) is solved using the second-order MUSCL-type (Monotonic Upstream-centered Scheme

for Conservation Laws) scheme, presented for instance in Chiapolino et al. (2017) and the HLLC-type Riemann solver introduced in Saurel et al. (2009). The interface-sharpening method of Chiapolino et al. (2017) is used as well with the help of the Overbee flux limiter. The time step is computed with a CFL number of 0.5.

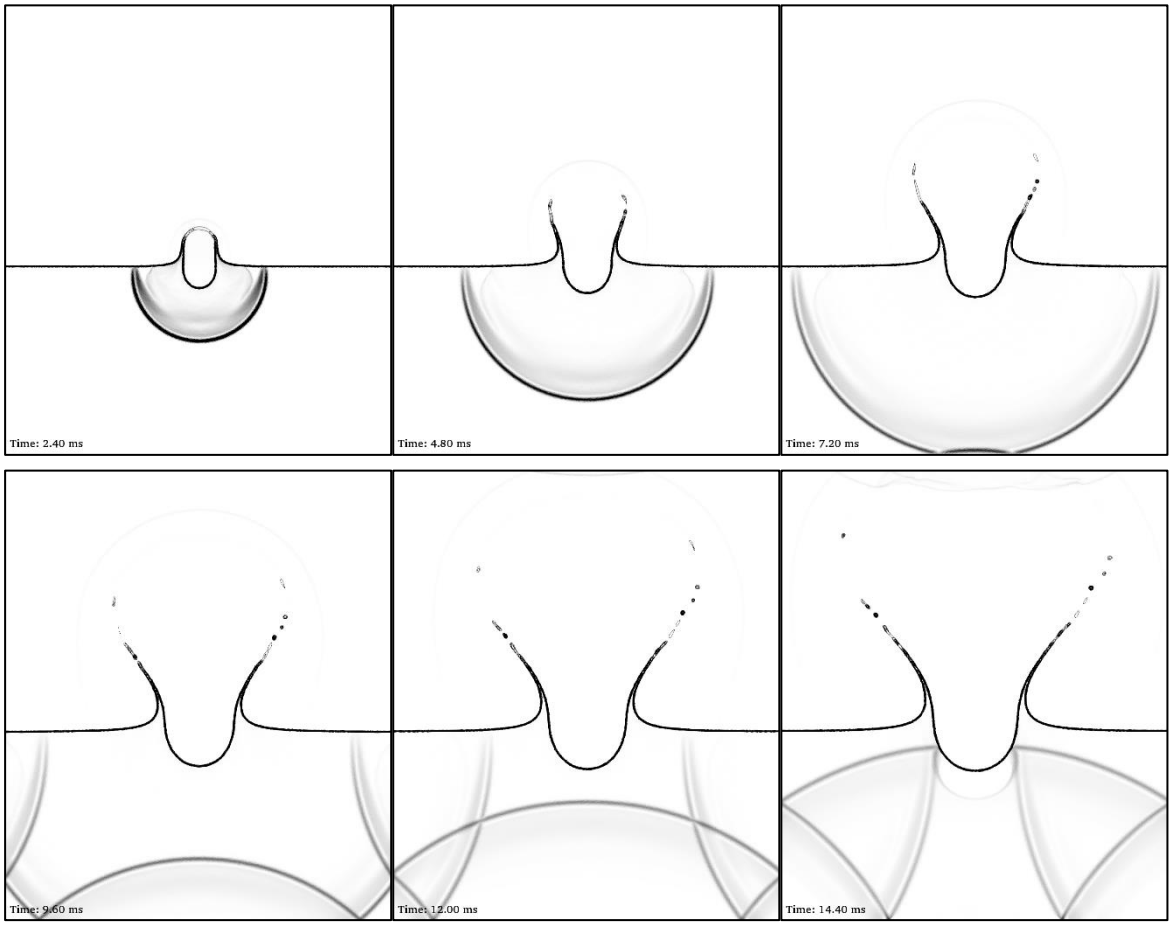

Figure 12. Two-dimensional underwater explosion test with the pressure non-equilibrium model of Saurel et al. (2009). Eight values of the liquid-volume-fraction isocontours are displayed within the range [0.1-0.9] in all figures. The mixture-pressure-gradient contours are displayed as well. Results are computed with the second-order MUSCL-type scheme and the interface-sharpening method presented in Chiapolino et al. (2017). The mesh consists of 356,620 unstructured triangles. The present thermodynamic relaxation method is used.

Due to the high-pressure gradient between the detonation products and the surrounding water, a strong shock is emitted into the water while an expansion wave propagates into the gas. The liquid-gas interface is set in intense motion and the bubble deforms. Another wave diffraction occurs at the liquid-air interface, resulting in the motion of the two liquid-gas interfaces. The bubble grows intensively, resulting in the appearance of a thin liquid layer between the air and the detonation products. This layer is stretched during time evolution and finally breaks into several fragments. No fragmentation model is introduced in the present computations. Effects of surface tension can be introduced, following Perigaud and Saurel (2005), but this is out of the scope of the present contribution.

Phase transition was not considered. However, the method is able to fragment a liquid film subjected to tension. Indeed, if the single-phase Euler equations were solved in the liquid, the pressure would be negative due to liquid tension. With the present diffuse-interface formulation (System 7.1), thanks to the small amount of air present in the liquid, sub-scale bubbles grow during pressure relaxation,

maintaining pressure positivity and resulting in the dynamic appearance of new interfaces that result in the formation of fragments. Such a break-up occurs automatically as a result of stretching (Saurel et al. 2009). This simplified modeling of cavitation is in principle representative enough in explosion situations such as the present case.

Pressure signals with and without the present thermodynamic relaxation method are compared in Figure 13.

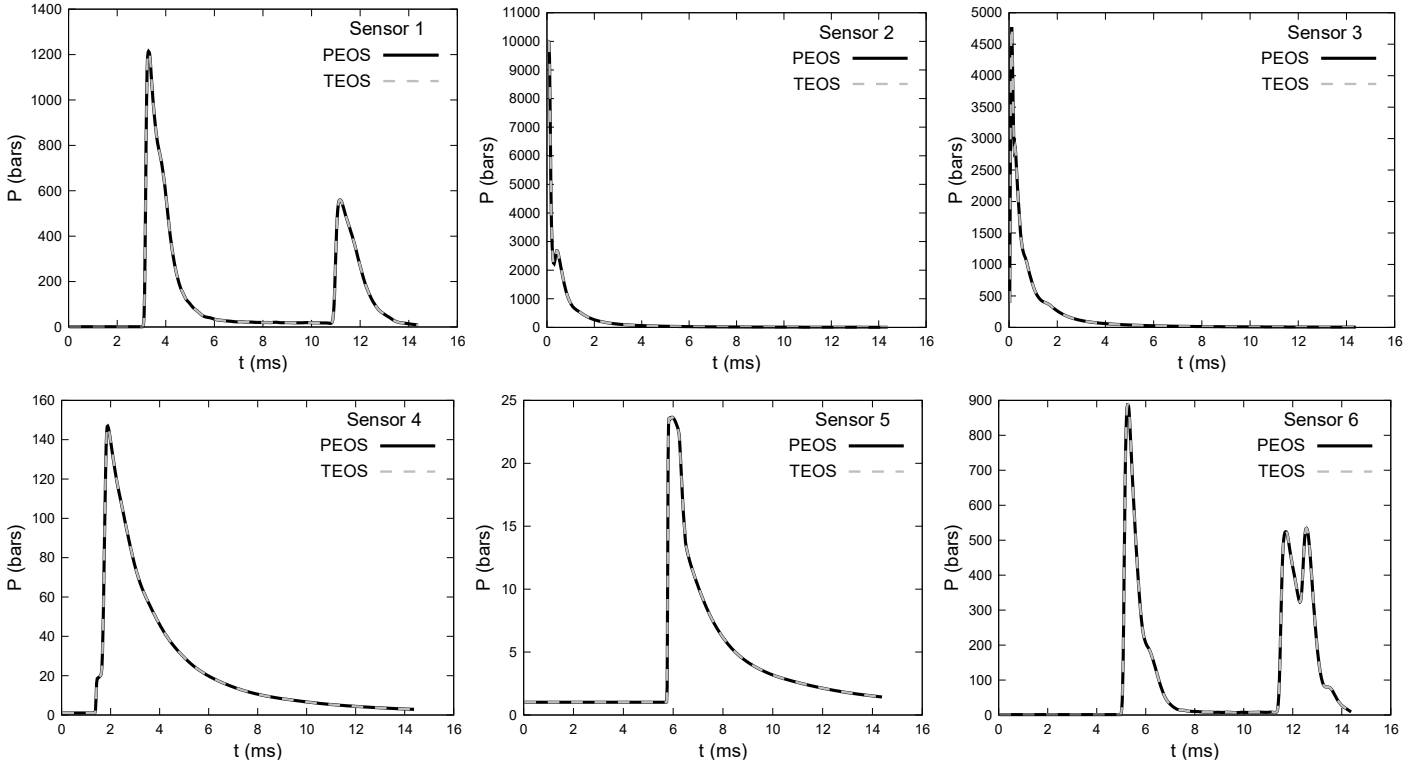

Figure 13. Two-dimensional underwater explosion test with the pressure non-equilibrium model of Saurel et al. (2009). Dashed gray lines represent computed results with the conventional method (TEOS), and black lines correspond to the relaxation method (PEOS). The results are compared in terms of mixture pressure with the help of the various sensors placed in the numerical domain (Figure 11). The present relaxation method perfectly recovers the target EOS results. The results are computed using the modified heat capacity of $C_v = 1000$ J.kg^{-1}.K^{-1} for the PBXN-109 detonation products, which provides easier numerical conditions, as seen in Appendix B.

The results computed with the relaxation method using the predictor EOS are merged with those obtained with the conventional method using the target EOS. Moreover, the use of the NASG expressions throughout the numerical code is computationally cheaper than with the JWL EOS. For the present test, parallel computations are run using MPI (Message Passing Interface) architecture and 60 CPUs. The TEOS simulation requires 35 minutes while the PEOS needs 21 minutes. The PEOS simulation is about 1.67 times faster than the TEOS simulation.

In the following, the same test is rerun with the actual heat capacity $C_v = 1960$ J.kg^{-1}.K^{-1} for the PBXN-109 detonation products, which is calculated from the thermochemical code Cheetah (see Yoh et al., 2005). In this situation, the conventional computation (TEOS) quickly fails as the third convexity condition of (4.15) is violated, indicating an unrealistic thermal expansion coefficient $\beta = \frac{1}{v}\frac{\partial v}{\partial T}\Big|_P$ and isothermal compressibility coefficient $\beta_T = -\frac{1}{v}\frac{\partial v}{\partial P}\Big|_T$, as seen in Section 4 via Eq.

(4.16). Failure occurs in numerical cells where the detonation-product phase is present in extremely small proportions and is subject to variations dictated by another phase, as discussed in Section 4.4. As the convexity criteria are no longer satisfied, the thermodynamic relaxation method (PEOS) omits the relaxation step, enabling the predictor EOS to carry out the computation. The results are compared in Figure 14.

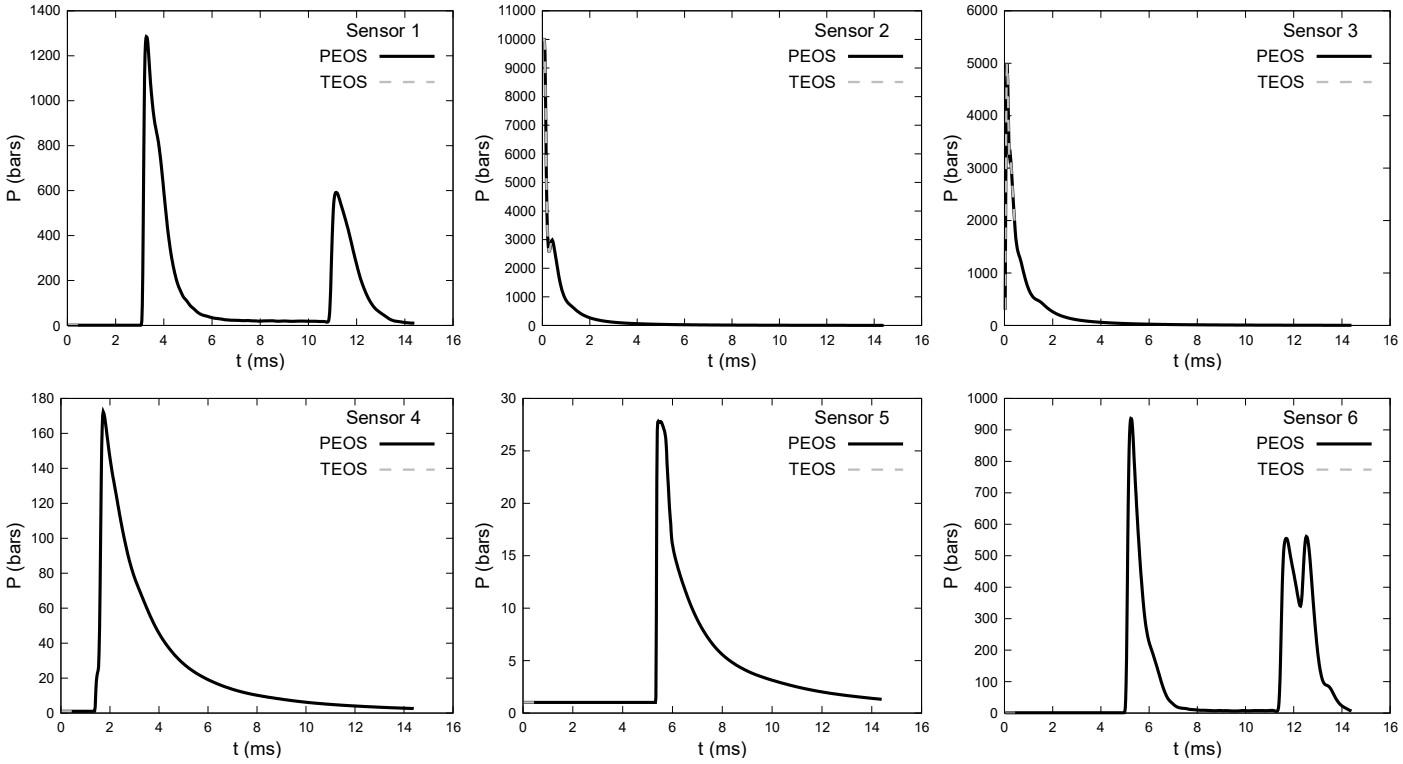

Figure 14. Two-dimensional underwater explosion test with the pressure non-equilibrium model of Saurel et al. (2009). Dashed gray lines represent computed results with the conventional method (TEOS), and black lines correspond to the relaxation method (PEOS). Pressure signals are compared at the various sensors placed in the numerical domain (Figure 11). The results are computed using the actual heat capacity of $C_v = 1960\ \text{J.kg}^{-1}.\text{K}^{-1}$ for the PBXN-109 detonation products. Beyond 0.45 ms, the conventional method (TEOS) fails while the relaxation method (PEOS) continues and completes the simulation.

The results indicate that at the early stages of the computations, the two methods (TEOS and PEOS) are merged. The PEOS method, with relaxation deactivated, continues while the TEOS method fails, and produces results consistent with those previously obtained.

8. Conclusion

A novel method has been developed to compute flows with sophisticated EOSs such as MG formulations. The present method has several key features:

- It automatically achieves the EOS prolongation that significantly improves the robustness of the computations, as most considered EOSs have a limited range of validity.
- It is 40% faster than computations achieved with the original EOS, in the multiphase flow examples considered herein.
- It is versatile, in the sense that various flow models can be considered with this method.

It is planned to extend the method to extra physics, such as cubic EOSs, as well as virial ones, each one having important interest in different technical areas.

In memoriam

This paper is dedicated to the memory of Sergei Konstantinovich Godunov.

Appendix A. Mayer relation for TEOS and PEOS

The derivations leading to Relation (4.3) $C_v^* = \dfrac{R^*}{\Gamma}$ are detailed in this appendix. The aim is to derive the relation of Mayer for both the TEOS and the PEOS. The general form of the relation of Mayer is,

$$C_p - C_v = T \left.\frac{\partial P}{\partial T}\right|_v \left.\frac{\partial v}{\partial T}\right|_p . \tag{A.1}$$

This thermodynamic relation is general in the sense that it is valid regardless of the equation of state (Nayigizente, 2021). The parameter C_p represents the specific heat at constant pressure. For the TEOS, with the help of Relations (2.1), the relation of Mayer (A.1) reads,

$$\frac{C_p}{C_v} - 1 = \Gamma. \tag{A.2}$$

Similarly, the relation of Mayer for the PEOS with Relations (3.1) is,

$$\frac{C_p^*}{C_v^*} - 1 = \frac{R^*}{C_v^*}. \tag{A.3}$$

The specific heat ratio $\gamma = C_p / C_v$ corresponds to the polytropic coefficient. Since both TEOS and PEOS aim to predict the same results for a given fluid, the polytropic coefficient is merged for both EOSs. Consequently, combining Relations (A.2) and (A.3) leads to,

$$C_v^* = \frac{R^*}{\Gamma}. \tag{A.4}$$

As $\Gamma = v \left.\dfrac{\partial p}{\partial e}\right|_v$ by definition, and as the specific volume v is provided by the flow model regardless of the equation of state, it implies,

$$\left.\frac{\partial P_{TEOS}}{\partial e}\right|_v = \left.\frac{\partial P_{PEOS}}{\partial e}\right|_v . \tag{A.5}$$

Appendix B. Convexity for TEOS

Convexity of an equation of state requires fulfillment of various criteria (Godunov et al., 1976, Menikoff and Plohr, 1989),

$$\begin{cases} \left.\dfrac{\partial^2 e}{\partial v^2}\right|_s > 0, \\ \left.\dfrac{\partial^2 e}{\partial s^2}\right|_v > 0, \\ \left.\dfrac{\partial}{\partial s}\right|_v \left.\dfrac{\partial e}{\partial v}\right|_s > 0, \\ \left.\dfrac{\partial^2 e}{\partial s^2}\right|_v \left.\dfrac{\partial^2 e}{\partial v^2}\right|_s - \left(\left.\dfrac{\partial}{\partial s}\right|_v \left.\dfrac{\partial e}{\partial v}\right|_s\right)^2 > 0, \end{cases} \tag{B.1}$$

where s represents the specific entropy. However, the formulation of the entropy may not always be practical to manipulate. To avoid such a complexity, the criteria (B.1) are reformulated without entropy. Calculations are based on the following two sets of relations.

- The Gibbs identity,

$$de = Tds - Pdv. \tag{B.2}$$

- The Maxwell relations (Callen and Kestin, 1960),

$$\begin{cases} \left.\dfrac{\partial T}{\partial v}\right|_s = -\left.\dfrac{\partial P}{\partial s}\right|_v, \\ \left.\dfrac{\partial T}{\partial P}\right|_s = \left.\dfrac{\partial v}{\partial s}\right|_P, \\ \left.\dfrac{\partial P}{\partial T}\right|_v = -\left.\dfrac{\partial s}{\partial v}\right|_T, \\ \left.\dfrac{\partial s}{\partial P}\right|_T = -\left.\dfrac{\partial v}{\partial T}\right|_P. \end{cases} \tag{B.3}$$

After various manipulations using (B.2) and (B.3), the convexity conditions (B.1) are rearranged as:

$$\begin{cases} \dfrac{c^2}{v^2} > 0, \\ \left.\dfrac{\partial T}{\partial p}\right|_{v_k} \left(\left.\dfrac{\partial e}{\partial v}\right|_T + p\right)\left(\left.\dfrac{\partial e}{\partial T}\right|_v\right)^{-1} > 0, \\ \left(\left.\dfrac{\partial e}{\partial v}\right|_T + p\right)\left(\left.\dfrac{\partial e}{\partial T}\right|_v\right)^{-1} > 0, \\ \left(\left.\dfrac{\partial e}{\partial v}\right|_T + p\right)\left(\left.\dfrac{\partial e}{\partial v}\right|_T\right)^{-2}\left(\dfrac{c^2}{v^2}\left.\dfrac{\partial e}{\partial p}\right|_v - \left.\dfrac{\partial e}{\partial v}\right|_T - p\right) > 0. \end{cases} \tag{B.4}$$

Inserting the general formulation of MG EOS (2.1) into (B.4) and after some simple algebraic manipulations, the set of convexity criteria (4.15) is obtained,

$$\begin{cases} P > P_k(v) + \dfrac{v}{\Gamma + 1}\dfrac{dP_k}{dv}, \\ P > P_k(v), \\ P > P_k(v) + v\dfrac{dP_k}{dv}. \end{cases} \tag{B.5}$$

These three relations imply the positivity of the squared speed of sound, the temperature, and the thermal expansion and isothermal compressibility coefficients respectively (see Section 4.4, Eqs. 4.15-4.16).

It is also worth mentioning that, applied to the JWL EOS, Relations (B.5) can be further manipulated by inserting the thermal EOS (second equation of Relations (2.1)) to obtain:

$$\begin{cases} \dfrac{C_v\Gamma(\Gamma+1)T}{v} - v\dfrac{dP_k}{dv} > 0, \\ \dfrac{C_v\Gamma T}{v} > 0, \\ C_v T\left(\dfrac{C_v\Gamma T}{v^2} - \dfrac{dP_k}{dv}\right) > 0. \end{cases} \tag{B.6}$$

Assuming that C_v, Γ, $v > 0$, the second inequality of Relations (B.6) implies $T > 0$ that consequently imposes $\dfrac{dP_k}{dv} < 0$ thanks to the first and third inequalities. This means that the function P_k must be strictly monotonically decreasing. Using Relations (2.4), one obtains:

$$\begin{aligned} & P_k(v)\searrow \;\Rightarrow\; Ae^{-R_1\frac{v}{v_{ref}}} + Be^{-R_2\frac{v}{v_{ref}}} + k\left(\frac{v_{ref}}{v}\right)^{\Gamma+1}\searrow \\ & A, B, R_1, R_2, v, v_{ref} > 0 \;\Rightarrow\; k > 0 \\ & \Rightarrow C_v < \frac{Cv_{CJ}}{\Gamma T_{CJ}}\left(\frac{v_{ref}}{v_{CJ}}\right)^{\Gamma+1} = \frac{\left(P_{CJ} - P_1(v_{CJ})\right)v_{CJ}}{\Gamma T_{CJ}} \end{aligned} \tag{B.7}$$

The JWL EOS is consequently convex as long as $T > 0$ under the strong constraint on C_v defined in Relation (B.7). However, this constraint may yield unrealistically low values for C_v and consequently inaccurate temperature predictions close to the Chapman-Jouguet point. Furthermore, a similar condition is not straightforward to derive for other MG-type EOSs such as the CC EOS.

Note that for the PBXN-109 detonation products used for the 2D underwater explosion test (Section 7), the JWL parameters provided in Table II yield,

$$C_v < \frac{v_{CJ}C}{\Gamma T_{CJ}}\left(\frac{v_{ref}}{v_{CJ}}\right)^{\Gamma+1} = 1032.15 \text{ J.kg}^{-1}.\text{K}^{-1}. \tag{B.8}$$

As the present 2D computation is only illustrative, $C_v = 1000 \text{ J.kg}^{-1}.\text{K}^{-1}$ is chosen to provide better numerical conditions, based on the previous observation.

Authors declarations

Conflicts of interest

The authors have no conflicts to disclose.

Authors contributions

Loann Neron: Conceptualization (equal); formal analysis (equal); methodology (equal); software (equal); visualization (equal); validation (equal); writing – original draft (equal); writing – review and editing (equal).

Richard Saurel: Conceptualization (equal); formal analysis (equal); methodology (equal); software (equal); visualization (equal); validation (equal); writing – original draft (equal); writing – review and editing (equal).

Alexandre Chiapolino: Conceptualization (equal); formal analysis (equal); methodology (equal); software (equal); visualization (equal); validation (equal); writing – original draft (equal); writing – review and editing (equal).

François Fraysse: Conceptualization (equal); formal analysis (equal); methodology (equal); software (equal); visualization (equal); validation (equal); writing – original draft (equal); writing – review and editing (equal).

Data availability

The data that supports the findings of this study are available within the article.

References

Abgrall, R., and Saurel, R., "Discrete equations for physical and numerical compressible multiphase mixtures," Journal of Computational Physics, 186(2), 361-396 (2003).

Arienti, M., Morano, E., and Shepherd, J. E., "Shock and detonation modeling with the Mie-Grüneisen equation of state," California Institute of Technology (2004).

Baer, M. R., and Nunziato, J. W., "A two-phase mixture theory for the deflagration-to detonation transition (DDT) in reactive granular materials," International Journal of Multiphase Flow, 12(6), 861-889 (1986).

Belkheeva, R. K., "Model of the Grüneisen coefficient for a wide range of densities on the example of copper," High Temperature, 60 (Suppl. 1), S26–S31 (2022).

Bushman, A.V., Lomonosov, I.V. and Khishchenko, K. V., "Shock wave data base," http://www.ficp.ac.ru/rusbank/ (2004).

Callen, H. B., and Kestin, J., "An Introduction to the Physical Theories of Equilibrium Thermostatics and Irreversible Thermodynamics," Wiley, New York (1960).

Chen, G. Q., Levermore, C. D., and Liu, T. P., "Hyperbolic conservation laws with stiff relaxation terms and entropy," Communications on Pure and Applied Mathematics, 47(6), 787-830 (1994).

Chiapolino, A., and Saurel, R., "Extended Noble-Abel stiffened-gas equation of state for sub-and-supercritical liquid-gas systems far from the critical point," Fluids, 3(3), 48 (2018).

Chiapolino, A., Saurel, R., and Nkonga, B., "Sharpening diffuse interfaces with compressible fluids on unstructured meshes," Journal of Computational Physics, 340, 389-417 (2017).

Chinnayya, A., Daniel, E., and Saurel, R., "Modelling detonation waves in heterogeneous energetic materials," Journal of Computational Physics, 196(2), 490-538 (2004).

Cocchi, J. P., Saurel, R., and Loraud, J. C., "Some remarks about the resolution of high velocity flows near low densities," Shock Waves, 8(2), 119-125 (1998).

Cochran, S. G. and Chan, J., "Shock initiation and detonation models in one and two dimensions," UCID-18024. California Univ., Livermore (1979).

Coquel, F., and Perthame, B. T., "Relaxation of energy and approximate Riemann solvers for general pressure laws in fluid dynamics," SIAM Journal on Numerical Analysis, 35(6), 2223-2249 (1998).

Davis, S. F., “Simplified Second-Order Godunov-Type Methods,” SIAM Journal on Scientific and Statistical Computing, 9(3) (1988).

Fried, L. E., Howard, W. M., and Souers, P. C., “Cheetah 2.0,” Lawrence Livermore National Laboratory, Livermore, CA, USA (1998).

Furfaro, D., and Saurel, R., “A simple HLLC-type Riemann solver for compressible non-equilibrium two-phase flows,” Computers & Fluids, 111, 159-178 (2015).

Godunov, S. K., “Finite difference method for numerical computation of discontinuous solutions of the equations of fluid dynamics,” Matematičeskij sbornik, 47(3), 271-306 (1959).

Godunov, S. K., Zabrodin, A. V., Ivanov, M. I., Kraiko, A. N., and Prokopov, G. P., “Numerical solution of multidimensional problems of gas dynamics,” Moscow Izdatel Nauka (1976).

Grove, J., and Menikoff, R., “Anomalous reflection of a shock wave at a fluid interface,” Journal of Fluid Mechanics, 219, 313–336 (1990).

Grüneisen, E., "Theorie des festen Zustandes einatomiger Elemente," Annalen der Physik 344 (12), 257–306 (1912).

Harten, A., Lax, P., and van Leer, B., “On Upstream Differencing and Godunov-Type Schemes for Hyperbolic Conservation Laws,” SIAM Review, 25 (1), 35–61 (1983).

Holt, M., “Underwater explosions,” Annual Review of Fluid Mechanics, 9 (1) 187-214 (1977).

Kapila, A. K., Menikoff, R., Bdzil, J. B., Son, S. F., and Stewart, D. S., “Two-phase modeling of deflagration-to-detonation transition in granular materials: Reduced equations,” Physics of fluids, 13(10), 3002-3024 (2001).

Le Métayer, O., and Saurel, R., “The Noble-Abel stiffened-gas equation of state,” Physics of Fluids, 28(4), 046102 (2016).

Le Métayer, O., Massoni, J., and Saurel, R., “Dynamic relaxation processes in compressible multiphase flows. Application to evaporation phenomena,” In Esaim: Proceedings (Vol. 40, pp. 103-123). EDP Sciences (2013).

Lee, E.L., Horning, H.C. and Kury, J.W., “Adiabatic Expansion of High Explosives Detonation Products,” Lawrence Radiation Laboratory, University of California, Livermore, TID 4500-UCRL 50422 (1968).

Levashov, P. R., Khishchenko, K. V., Lomonosov, I. V., and Fortov, V. E., “Database on shock-wave experiments and equations of state available via Internet,” AIP Conf. Proc., 706, 87–90 (2004).

Levermore, C. D., "Moment closure hierarchies for kinetic theories," Journal of statistical Physics, 83, 1021-1065 (1996).

Liu, T.P., “Hyperbolic conservation laws with relaxation,” Communications in Mathematical Physics 108, 153-175 (1987).

Lomonosov, I. V., and Fortova, S. V., “Wide-range semiempirical equations of state of matter for numerical simulation on high-energy processes,” High Temperature, 55 (4), 585-610 (2017).

Lund, H., “A hierarchy of relaxation models for two-phase flow,” SIAM Journal on Applied Mathematics, 72-6), 1713-1741 (2012).

Maire, P. H., and Nkonga, B., “Multi-scale Godunov-type method for cell-centered discrete Lagrangian hydrodynamics,” Journal of Computational Physics, 228(3), 799-821 (2009).

Marsh, S.P., “LASL Shock Hugoniot Data,” University of California Press (1980).

Massoni, J., Saurel, R., Lefrançois, A., and Baudin, G., “Modeling spherical explosions with aluminized energetic materials,” Shock Waves (16), 75-92 (2006).

Menikoff, R., and Plohr, B. J., “The Riemann problem for fluid flow of real materials,” Reviews of modern physics, 61(1), 75 (1989).

Menikoff, R., “JWL equation of state,” No. LA-UR-15-29536. Los Alamos National Lab. (LANL), Los Alamos, NM (United States), (2015).

Mie, G., “Zur kinetischen Theorie der einatomigen Körper,” Annalen der Physik 316 (8), 657–697 (1903).

Miller, G. H., and Puckett, E. G., “A high-order Godunov method for multiple condensed phases,” Journal of Computational Physics, 128(1), 134-164 (1996).

Nayigizente, D., “Unsteady simulations of liquid/gas interfaces in real gas flows using the Second Gradient theory: Simulations instationnaires d’interfaces liquide/gaz dans les écoulements gaz réels en utilisant la théorie du Second Gradient,” Doctoral dissertation, Université Paris- Saclay (2021).

Neron, L., and Saurel, R., “Noble–Abel/first-order virial equations of state for gas mixtures resulting from multiple condensed reactive materials combustion,” Physics of Fluids, 34(1), 016107 (2022).

Perigaud, G., and Saurel, R., “A compressible flow model with capillary effects,” Journal of Computational Physics, 209(1), 139-178 (2005).

Plohr, B.J., “Shockless acceleration of thin plates modeled by a tracked random choice method,” AIAA Journal, 26(4), 470-478 (1988).

Povarnitsyn, M. E., Khishchenko, K. V., and Levashov, P. R., “Hypervelocity impact modeling with different equations of state,” Int. J. Impact Eng., 33 (1–12), 625–633 (2006).

Saurel, R., and Abgrall, R., “A multiphase Godunov method for compressible multifluid and multiphase flows,” Journal of Computational Physics, 150(2), 425-467 (1999a).

Saurel, R., and Abgrall, R., “A simple method for compressible multifluid flows,” SIAM Journal on Scientific Computing, 21(3), 1115-1145 (1999b).

Saurel, R., and Pantano, C., “Diffuse-interface capturing methods for compressible two-phase flows,” Annual Review of Fluid Mechanics, 50, 105-130 (2018).

Saurel, R., Franquet, E., Daniel, E., and Le Métayer, O., “A relaxation-projection method for compressible flows. Part I: The numerical equation of state for the Euler equation,” Journal of Computational Physics 223, 822-845 (2007b).

Saurel, R., Fraysse, F., Furfaro, D., and Lapebie, E., “Reprint of: Multiscale multiphase modeling of detonations in condensed energetic materials,” Computers & Fluids, 169, 213-229 (2018).

Saurel, R., Gavrilyuk, S., and Renaud, F., “A multiphase model with internal degrees of freedom: Application to shock-bubble interaction,” Journal of Fluid Mechanics, 495, 283-321 (2003).

Saurel, R., Larini, M., and Loraud, J. C., “Exact and Approximate Riemann Solvers for Real Gases,” Journal of Computational Physics, 112(1), 126-137 (1994).

Saurel, R., Le Martelot, S., Tosello, R., and Lapébie, E., “Symmetric model of compressible granular mixtures with permeable interfaces,” Physics of Fluids, 26(12) (2014).

Saurel, R., Le Métayer, O., Massoni, J., and Gavrilyuk, S., “Shock jump relations for multiphase mixtures with stiff mechanical relaxation,” Shock waves, 16(3), 209-232 (2007a).

Saurel, R., Petitpas, F., and Berry, R. A., “Simple and efficient relaxation methods for interfaces separating compressible fluids, cavitating flows and shocks in multiphase mixtures,” Journal of Computational Physics, 228(5), 1678-1712 (2009).

Souers, P. C., Anderson, S., Mercer, J., McGuire, E., and Vitello, P., “JWL++: a simple reactive flow code package for detonation,” Propellants, Explosives, Pyrotechnics, 25(2), 54-58 (2000).

Sućeska, M., “Evaluation of detonation energy from EXPLO5 computer code results,” Propellants, Explosives, Pyrotechnics, 24(5), 280-285 (1999).

Toro, E. F., “Riemann solvers and numerical methods for fluid dynamics: A practical introduction,” Springer Science & Business Media (1999).

Toro, E. F., “Some IVP’s for which conservative methods fail miserably,” Proceedings of the 6th International Symposium on Comput. Fluid Dynamics, Lake Tahoe, CA (1995).

Toro, E. F., Spruce, M., and Speares, W., “Restoration of the contact surface in the HLL-Riemann solver,” Shock waves, 4, 25-34 (1994).

Udaykumar, H. S., Tran, L., Belk, D. M., and Vanden, K. J., “An Eulerian method for computation of multimaterial impact with ENO shock-capturing and sharp interfaces,” Journal of Computational Physics, 186(1), 136-177 (2003).

Van der Waals, J. D., “Over de Continuiteit van den Gas-en Vloeistoftoestand (Vol. 1),” Sijthoff (1873).

Yoh, J. J., McClelland, M. A., Maienschein, J. L., Wardell, J. F., and Tarver, C.M., “Simulating thermal explosion of cyclotrimethylenetrinitramine-based explosives: Model comparison with experiment,” Journal of Applied Physics, 97, no. 8 (2005).